NEUROSCIENCE

A circuit from dorsal hippocampal CA3 to parvafox nucleus mediates chronic social defeat stress–induced deficits in preference for social novelty

Yang Liu[1]†, Si-Long Deng[1]†, Liang-Xia Li[1], Zi-Xiang Zhou[1], Qiu Lv[1], Zhong-Yuan Wang[1], Fang Wang[1,2,3]*, Jian-Guo Chen[1,2,3]*

The preference for social novelty is crucial to the social life of humans and rodents. However, the neural mechanisms underlying social novelty preference are poorly understood. Here, we found that chronic social defeat stress (CSDS) reduced the preference for social novelty in mice by impairing the response of CaMKIIα$^+$ neurons in the CA3 region of dorsal hippocampus (dCA3) during approach to an unfamiliar mouse. The deficits of social novelty preference in CSDS-treated mice were reversed by activating the output from dCA3 to the GABAergic neurons in the lateral septum (LS). The activation of GABAergic projection from LS recruited a circuit that inhibited the Foxb1$^+$ neurons in the parvafox nucleus (PFN), which drove social avoidance by projecting to the lateral periaqueductal gray (lPAG). These results suggest that a previously unidentified circuit of dCA3$^{CaMKII\alpha+}$→LS^{GABA+}→PFN^{Foxb1+}→lPAG mediates the deficits of social novelty preference induced by CSDS.

INTRODUCTION

Social behavior is a broad term encompassing many types of interactions between individuals of the same species. However, a fundamental prerequisite of a wide range of these behaviors is believed to be social recognition, the ability of an animal to identify another individual's familiarity (*1*). The preference for social novelty is defined as a notable propensity to spend more time with an unfamiliar mouse than with a familiar mouse (*2*). The deficits in the preference for social novelty are commonly associated with neuropsychiatric disease (*3*); for example, the impairment of social novelty preference in juvenile is an important early marker for autism (*2*).

The social recognition memory of rodents is dependent on the integrity of the hippocampus (*4*). Anatomically, the structure has been classically defined as a circuit that processes social information arriving from the entorhinal cortex (EC) sequentially through the dentate gyrus (DG), CA3, and CA1 subfields (*5*). Previous studies have shown that activity in ventral CA3 (vCA3), but not dorsal CA3 (dCA3), is necessary for the encoding of social memory (*6*). Donegan *et al.* (*7*) found a crucial role for CA2 in the normal encoding of social stimuli. However, available data do not support the idea that they are the direct and key factors driving the preference for social novelty. Alternatively, increasing evidence indicates that the dCA3 could be activated by stimulation of unfamiliar mice and control social approach behavior (*6*, *8*), suggesting that dCA3 may directly participate in the preference for social novelty.

Low level of social novelty preference and excessive avoidance often occur in parallel (*9*). While the expression of social novelty preference is considered to be instinctive, their magnitude and susceptibility may be affected by environmental factors and internal balance of social approach-avoidance (*10*). Chronic social defeat stress (CSDS) in rodents has been recently used to study the neural circuitry underlying social behaviors (*11*). It is believed that the activity of neural circuit can be reconfigured by social stress to produce a variety of outputs and suppress the social approach behaviors (*11*, *12*). However, the related neural circuit mechanism underlying the deficits of social novelty preference induced by CSDS is still largely unknown.

Similar to aggressive behavior, the preference for social novelty also requires the social encounter and decision-making process (*13*). Previous studies have shown that both dCA3 and dCA2 are involved in the regulation of social behavior through the projection to the lateral septum (LS) (*14*). dCA3 is an important brain area that responds to social defeat stress (*15*). The dCA3 contains mainly Ca^{2+}/calmodulin-dependent protein kinase II α subtype (CaMKIIα)–positive pyramidal neurons (*16*). Chronic exposure to social defeat has been found to induce the changes in dCA3$^{CaMKII\alpha+}$ neurons (*17*). The neural circuitry of dCA3→LS participates in the context-associated memory (*18*). LS is an important component of the neural circuit mediating the expression of social behavior (*19*). Furthermore, LS^{GABA+} neurons have been reported to be involved in the regulation of social behaviors such as avoidance and aggression (*20*, *21*). On the other hand, the murine parvafox nucleus (PFN) that consists of forkhead box protein b1 (Foxb1)–expressing neurons appears to correspond partially to the paraterete hypothalamic nucleus and to be contained within the magnocellular nucleus of the lateral hypothalamus (*22*, *23*). Bilella *et al.* (*24*) found that the PFN^{Foxb1+} neurons regulated the defensive reaction to life-threatening situations, suggesting that these neurons are involved in instinctive behaviors.

In the present study, we found that activation of a cell-specific circuit of dCA3$^{CaMKII\alpha+}$→dorsal LS^{GABA+}→PFN^{Foxb1+} reversed the deficits of social novelty preference in defeated mice, and inhibition of this circuit reduced the preference for social novelty. The circuit that regulated the preference for social novelty may serve as an important mechanism of emotion and the development of affective disorders.

[1]Department of Pharmacology, Tongji Medical College, Huazhong University of Science and Technology, Wuhan 430030, China. [2]The Key Laboratory of Neurological Diseases (HUST), Ministry of Education of China, Wuhan 430030, China. [3]The Key Laboratory for Drug Target Researches and Pharmacodynamic Evaluation of Hubei Province, Wuhan 430030, China.
*Corresponding author. Email: chenj@mails.tjmu.edu.cn (J.-G.C.); wangfanghust@hust.edu.cn (F.W.)
†These authors contributed equally to this work.

RESULTS

CSDS reduces the preference for social novelty in mice

CSDS paradigm can induce social deficits and has been widely used in affective disorder research (*25*). As shown in Fig. 1A, naïve C57BL/6J (C57) mice were introduced into the home cage of an unfamiliar CD1 aggressor mouse, and they were allowed to interact for 10 min daily over 10 consecutive days, and then the C57 mice were tested in a social interaction test (SIT) to assess social behavior. C57 mice were separated into susceptible and resilient subpopulations according to the sniffing time (Fig. 1, B and C). Susceptible mice displayed a significant decrease in the sniffing time with an unfamiliar CD1 mouse (Fig. 1D), while control mice were not exposed to the stressful experience of social defeat. In a three-chamber test with an unfamiliar CD1 mouse versus an empty cage, we also found that the preference for an unfamiliar CD1 mouse was decreased in susceptible mice (fig. S1A). Considering that CD1 and C57 mice are two different strains of mice, we used various types of three-chamber tests based on the natural tendency for mice to evaluate social preference (sociability) and social novelty preference in mice. We found that the preference for familiar mice was not affected by CSDS in the three-chamber test with a familiar C57 mouse versus a novel object (Fig. 1, E and F). However, in the social novelty task,

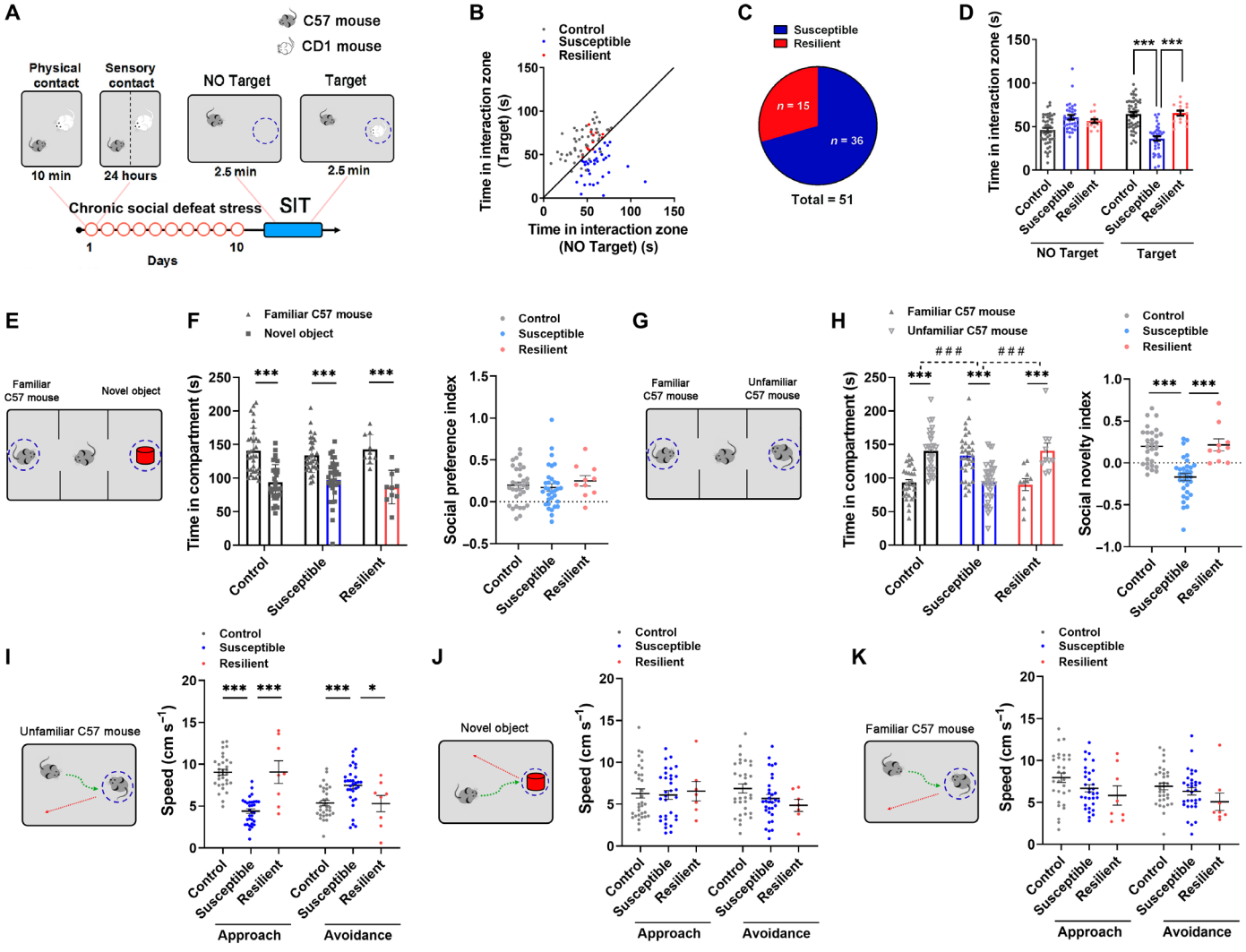

Fig. 1. CSDS reduces the preference for social novelty in mice. (**A**) Schematic diagram of the CSDS procedure and behavior test. (**B**) Scatterplots of duration in the no target interaction zone and target interaction zone for control, susceptible, and resilient mice (black diagonal line, no target interaction time = target interaction time). (**C**) The proportion of susceptible (70.59%, $n = 36$) and resilient (29.41%, $n = 15$) mice produced by exposure to CSDS. (**D**) The susceptible mice showed less sniffing time in the interaction zone (target). (**E**) Schematic diagram of the three-chamber test with a familiar C57 mouse versus a novel object. (**F**) Left: The time spent in the compartments with a novel object or a familiar C57 mouse. Right: The social preference index of susceptible mice was unchanged. (**G**) Schematic diagram of the three-chamber test with a familiar C57 mouse versus an unfamiliar C57 mouse. (**H**) Left: Time in the compartment with an unfamiliar C57 mouse was decreased in susceptible mice. Repeated-measures two-way ANOVA followed by Bonferroni's comparisons test, with asterisks depicting familiar C57 mouse versus unfamiliar C57 mouse comparisons, and the dashed line depicting comparisons between control versus susceptible and resilient versus susceptible in the presence of an unfamiliar C57 mouse. Right: Scatterplot depicting the decrease in social novelty index of susceptible mice. (**I** to **K**) The approach speed of susceptible mice was decreased and the avoidance speed was increased in susceptible mice when targeting an unfamiliar C57 mouse (I) but not a novel object (J) or a familiar C57 mouse (K). Data are expressed as means ± SEM. ###$P < 0.001$, *$P < 0.05$, and ***$P < 0.001$.

the preference for the unfamiliar C57 mouse was impaired in susceptible mice (Fig. 1, G and H), indicating that CSDS causes the deficit in the preference for social novelty but not in sociability.

By measuring the speed of mice in SIT (fig. S2, A to D), we found that the susceptible mice showed a greater velocity moving away from the unfamiliar CD1 mouse. Meanwhile, the approach speed was reduced in susceptible mice, suggesting that the approach-avoidance balance is changed by CSDS (fig. S1B). To investigate whether the deficits of approach-avoidance were general, we also measured the approach-avoidance velocities when targeting a novel object or a familiar or unfamiliar C57 mouse, respectively. We found that susceptible mice displayed decreased approach speed and increased avoidance speed when targeting an unfamiliar C57 mouse but not a novel object or familiar C57 mouse (Fig. 1, I to K), indicating that the approach-avoidance balance impaired by CSDS is individually addressed to an unfamiliar mouse but not general social situations. Next, the susceptible mice were selected and treated as the CSDS group for subsequent experiments.

The response of dCA3$^{CaMKII\alpha+}$ neurons during approach to an unfamiliar mouse is impaired by CSDS

Previous studies have shown that dCA3 is involved in the regulation of social recognition. To investigate the role of dCA3 in the preference for social novelty, the expression of immediate early gene c-Fos was examined. It was shown that the neurons in the pyramidal layer of dCA3 were more activated when exposed to an unfamiliar C57 mouse than to a familiar C57 mouse or a novel object (Fig. 2, A and B). We next used in vivo fiber photometry to examine the real-time activity of dCA3$^{CaMKII\alpha+}$ neurons during social approach. A genetically encoded calcium indicator GCaMP6m in adeno-associated virus (AAV) vector driven by the CaMKIIα promoter (AAV-CaMKIIα-GCaMP6m-WPREs-pA) was bilaterally microinjected into the dCA3 of mice to achieve CaMKIIα^{+} neuron–specific expression of GCaMP6m (Fig. 2C) (*26*). To assess how the dCA3$^{CaMKII\alpha+}$ neurons were activated during social approach, the duration of approach to an empty cage, a novel object, a familiar C57 mouse, and an unfamiliar C57 mouse in every trial was recorded. The dCA3$^{CaMKII\alpha+}$ neurons expressing the calcium indicator GCaMP6m in control mice were more robustly activated when approaching an unfamiliar C57 mouse compared with that in other groups (Fig. 2, D to G). However, the response of dCA3$^{CaMKII\alpha+}$ neurons during approach to an unfamiliar C57 mouse was impaired in CSDS-treated mice (Fig. 2, H to K, and fig. S3, A to L). The same effect was observed during approach to an unfamiliar CD1 mouse (fig. S4, A to N), demonstrating that dCA3$^{CaMKII\alpha+}$ neurons respond to an unfamiliar mouse during approach, and this response is impaired following CSDS.

Considering that the neuronal activity of dCA3 was decreased in CSDS-treated mice, we asked whether the excitability of dCA3$^{CaMKII\alpha+}$ neurons could be altered by social deficits. First, the mice were microinjected with AAV-CaMKIIα-EYFP-WPREs-pA into the dCA3 region. After 3 weeks, the mice were exposed to CSDS. Then, the whole-cell patch-clamp recordings were performed on acute hippocampal slices to examine the changes in the electrophysiology of the enhanced yellow fluorescent protein (EYFP)-positive cells in control and CSDS groups. We found that CSDS did not alter the resting membrane potential of these cells compared with that in the control group (Fig. 2L). However, exposure to CSDS decreased the number of action potentials evoked by injection of depolarizing currents (500-ms duration, 0 to 300 pA, 50-pA steps) compared with that of the control group (Fig. 2, M and N). Furthermore, we observed an increased threshold to induce the first spike in response to current injection in the CSDS group (Fig. 2, O and P), indicating that repeated exposures to social defeat decrease the excitability of dCA3$^{CaMKII\alpha+}$ neurons.

Manipulations of dCA3$^{CaMKII\alpha+}$→dLS projection activity regulate the preference for social novelty in mice

To gain an insight into projections from the dCA3$^{CaMKII\alpha+}$ neurons, the extrahippocampal projections were examined by locally injecting into dCA3 with AAV-CaMKIIα-NpHR3.0-EYFP-WPREs-pA. We observed the dense fibers in the dLS from dCA3$^{CaMKII\alpha+}$ neurons (Fig. 3, A and B). To eliminate the influence of stress vulnerability on behavior, we added a subthreshold social defeat stress (SSDS) (*27*) group and found that SSDS did not affect the preference for social novelty of C57 mice (fig. S5, A to J). To examine whether the activity of dCA3$^{CaMKII\alpha+}$→dLS projection neurons was necessary for social novelty preference, we used a dual-virus approach to chemogenetically silence the dCA3$^{CaMKII\alpha+}$→dLS projection neurons. Canine adenovirus-2 encoding Cre recombinase (CAV2-CMV-Cre) was infused into the dLS, and a Cre-dependent AAV expressing DREADD (hM4Di) was infused into the dCA3 (fig. S6A). We chemogenetically silenced dCA3$^{CaMKII\alpha+}$→dLS projection neurons that express hM4Di. Silence of dCA3$^{CaMKII\alpha+}$→dLS projection neurons through clozapine *N*-oxide (CNO) dihydrochloride treatment reduced the preference for social novelty in both control and SSDS-treated mice (fig. S6, B to G). This manipulation also reduced the approach speed and enhanced the avoidance speed when targeting an unfamiliar C57 mouse or CD1 mouse in both groups (fig. S6, H to K). Chemogenetic silence of dCA3$^{CaMKII\alpha+}$→dLS projection neurons also reduced social preference for the unfamiliar CD1 mouse in the SSDS group (fig. S6, L to N).

To rule out the possibility that our observed results were due to inhibition of collateral projections to other brain areas, we optogenetically suppressed the activity of dCA3$^{CaMKII\alpha+}$ projection terminals in the dLS. dCA3$^{CaMKII\alpha+}$→dLS projection terminals virally expressing the inhibitory opsin NpHR3.0 under the CaMKIIα promoter were illuminated by a continuous yellow laser (589 nm, 10 mW) over the dLS during behavior testing. In the social novelty task, optogenetic inhibition of dCA3$^{CaMKII\alpha+}$→dLS projection reduced the preference for the unfamiliar mouse versus a familiar mouse in both control and SSDS groups (Fig. 3, C to E). However, in the sociability task, this manipulation produced no effect on the preference for a familiar mouse versus a novel object (Fig. 3, F to H). In a social approach-avoidance speed test, we also found that optogenetic inhibition of dCA3$^{CaMKII\alpha+}$→dLS projection led to the decrease in approach speed and increase in the avoidance speed when targeting an unfamiliar C57 mouse or unfamiliar CD1 mouse but not a familiar C57 mouse or novel object in both control and SSDS-treated mice (Fig. 3, I and J, and fig. S7, A and B). This manipulation also reduced social preference for the unfamiliar CD1 mouse in the SSDS group (fig. S7, C to E), without effect on anxiety-related or motor behaviors in an open-field test (OFT) and tail suspension test (TST) (fig. S7, F and G). Collectively, these results demonstrate that the activity of dCA3$^{CaMKII\alpha+}$→dLS projection is involved in the preference for social novelty.

To examine whether increased activity of dCA3$^{CaMKII\alpha+}$→dLS projection was sufficient to rescue the preference for social novelty of CSDS-treated mice, the dCA3$^{CaMKII\alpha+}$→dLS projection virally expressing channelrhodopsin-2 (ChR2) under the CaMKIIα promoter

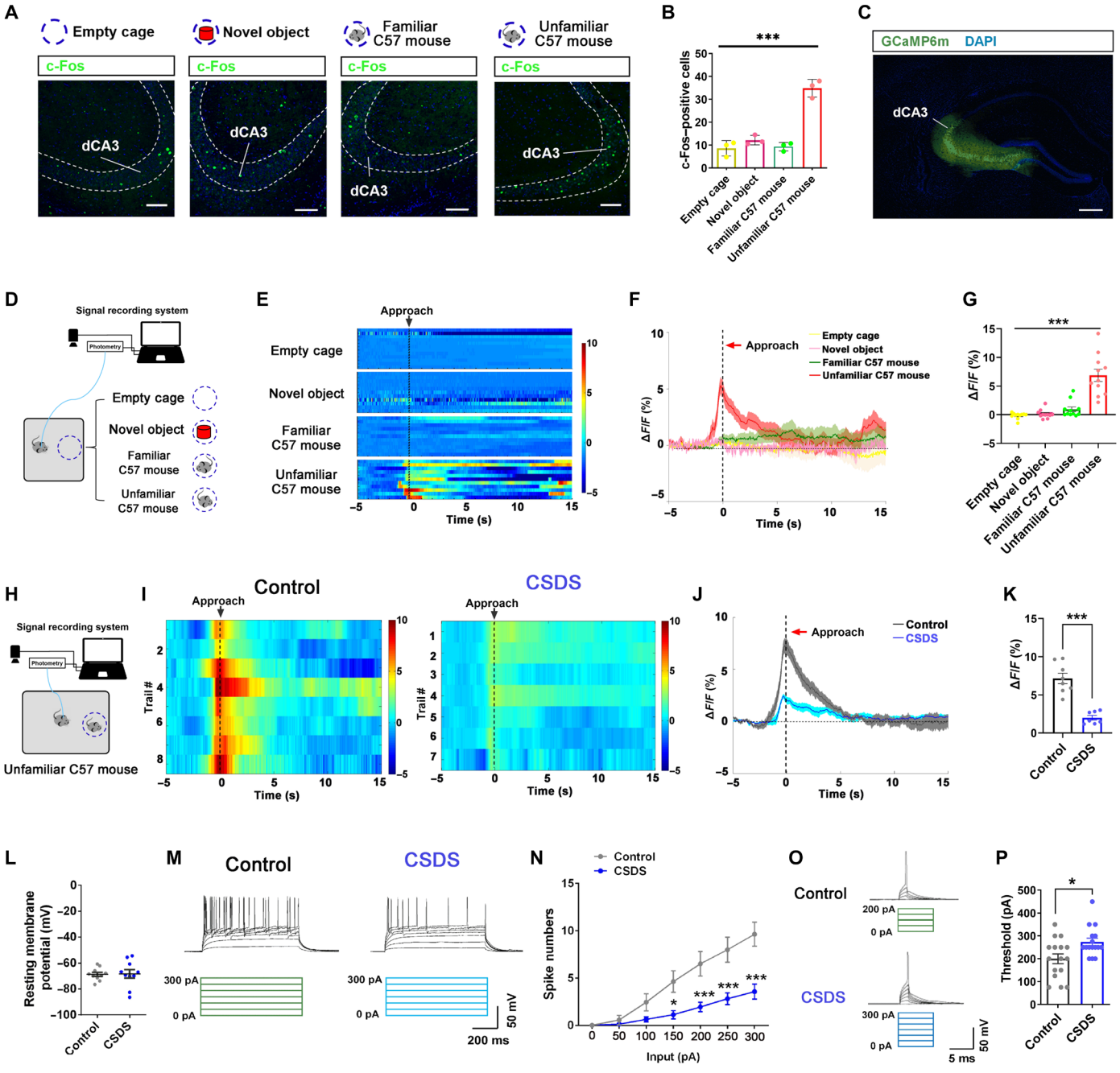

Fig. 2. CSDS impairs the responses of dCA3$^{CaMKII\alpha+}$ neurons during approach to an unfamiliar C57 mouse. (**A**) Representative images of c-Fos immunofluorescence in dCA3 region after social exposure. Scale bars, 100 μm. (**B**) Numbers of dCA3 c-Fos$^+$ cells in control mice were increased after exposure to an unfamiliar C57 mouse compared with those in other groups. (**C**) Representative photomicrographs of GCaMP6m expression in dCA3. Scale bar, 500 μm. (**D**) Schematic diagram of the fiber photometry recording. (**E**) Representative heatmaps of calcium transients evoked by approaching an unfamiliar C57 mouse. Color scales at the right indicating Δ*F*/*F*. (**F**) Average calcium transients evoked by approaching an unfamiliar C57 mouse but not in other groups. Shaded areas around means indicating error bars. (**G**) The peak calcium transients at the onset of approaching an unfamiliar C57 mouse were increased. (**H**) Schematic diagram of the fiber photometry recording in control and CSDS-treated mice. (**I**) Heatmaps of calcium transients evoked by approaching an unfamiliar C57 mouse from control and CSDS-treated mice. Color scales at the right indicating Δ*F*/*F*. (**J**) Average calcium transients of the control and CSDS-treated mice. Shaded areas around means indicating error bars. (**K**) The peak calcium transients at the onset of approaching an unfamiliar C57 mouse were increased in the control group but not in the CSDS group. (**L**) The resting membrane potential of dCA3$^{CaMKII\alpha+}$ neurons was not altered by social defeats. (**M** and **N**) The current-induced spike numbers in dCA3$^{CaMKII\alpha+}$ neurons were decreased with current (0 to 300 pA, 50-pA steps) injections in CSDS-treated mice. (**O** and **P**) Representative traces (O) and scatterplot (P) depicting the threshold currents required for action potential firing in dCA3$^{CaMKII\alpha+}$ neurons of control and CSDS-treated mice. Data are expressed as means ± SEM. **P* < 0.05 and ****P* < 0.001.

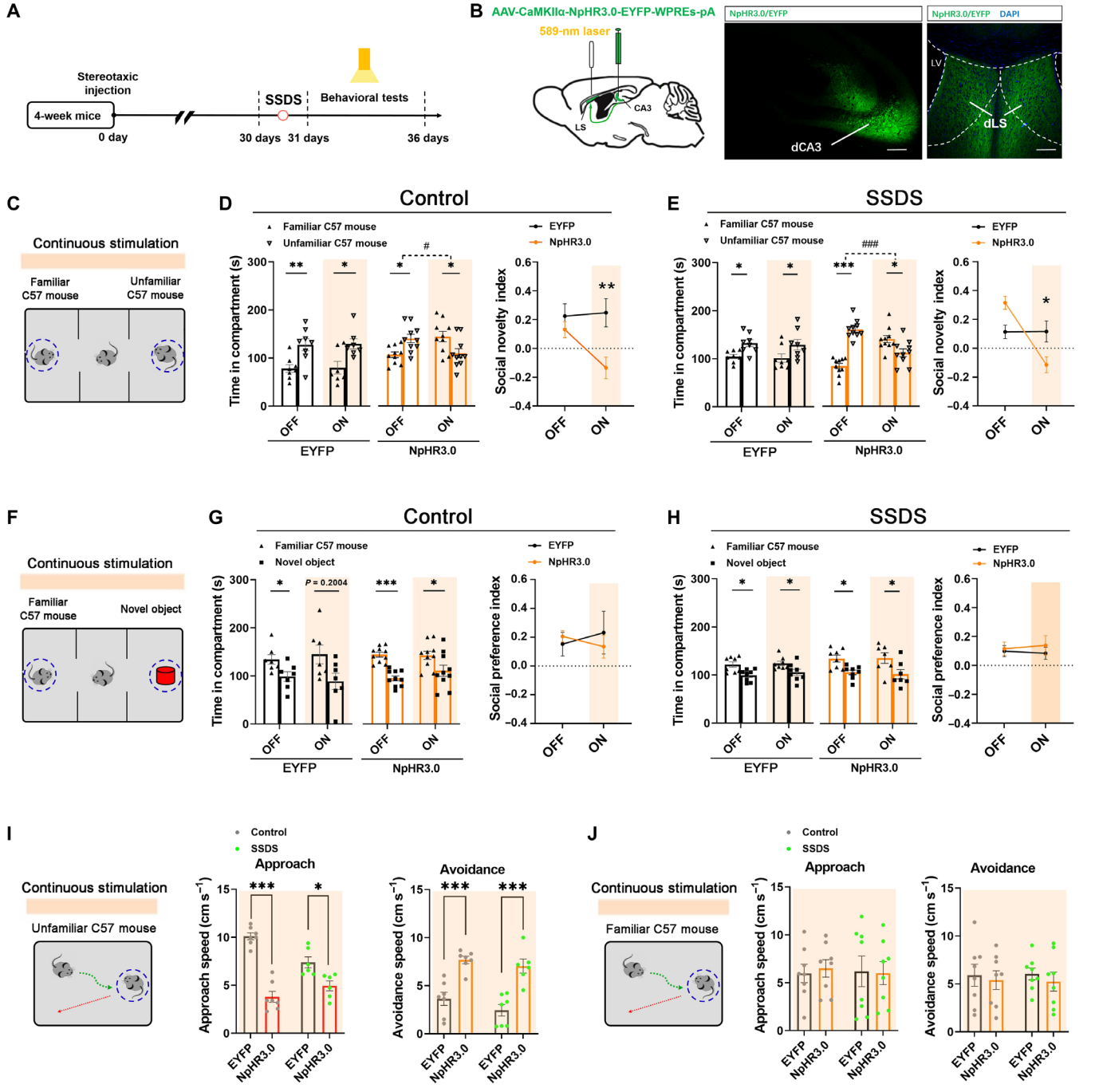

Fig. 3. Optogenetic inhibition of dCA3$^{CaMKII\alpha+}$→dLS projection reduces the preference for social novelty in mice. (**A**) Schematic experimental timeline of optogenetic inhibition experiments. (**B**) Left: Mice were injected into the dCA3 region with AAV and implanted above the dLS with optical fibers. Right: Representative immunofluorescence images of NpHR3.0-EYFP in dCA3$^{CaMKII\alpha+}$ neurons and dLS terminals. Scale bars, 250 μm (dCA3) and 100 μm (dLS). (**C**) Schematic diagram of optogenetic inhibition during the three-chamber test with a familiar C57 mouse versus an unfamiliar C57 mouse. (**D** and **E**) Optogenetic inhibition of dCA3$^{CaMKII\alpha+}$→dLS reduced the time spent in the compartment with an unfamiliar C57 mouse and social novelty index in both control (D) and SSDS-treated (E) mice. Repeated-measures two-way ANOVA followed by Bonferroni's comparisons test, with asterisks depicting familiar C57 mouse versus unfamiliar C57 mouse comparisons, and the dashed line depicting comparisons between OFF and ON in the NpHR3.0 condition. (**F**) Schematic diagram of optogenetic inhibition during the three-chamber test with a familiar C57 mouse versus a novel object. (**G** and **H**) Optogenetic inhibition of dCA3$^{CaMKII\alpha+}$→dLS projection produced no change in the time spent in the compartment with a familiar C57 mouse and social preference index in both control (G) and SSDS-treated (H) mice. (**I**) Left: Schematic diagram of optogenetic inhibition during the approach-avoidance speed test with an unfamiliar C57 mouse. Right: Optogenetic inhibition of dCA3$^{CaMKII\alpha+}$→dLS projection reduced the approach speed and increased the avoidance speed in both control and SSDS-treated mice. (**J**) Left: Schematic diagram of optogenetic inhibition during the approach-avoidance speed test with a familiar C57 mouse. Right: The approach speed and avoidance speed were unchanged by inhibition of dCA3$^{CaMKII\alpha+}$→dLS projection in both control and SSDS-treated mice. Data are expressed as means ± SEM. #$P < 0.05$, ###$P < 0.001$, *$P < 0.05$, **$P < 0.01$, and ***$P < 0.001$. LV, lateral ventricle.

was optogenetically activated by illuminating a blue laser beam (20 Hz, 5-ms pulse, 10 mW) over the dLS while mice performed the behavior tests (Fig. 4, A and B). It was shown that optogenetic activation of dCA3$^{CaMKII\alpha+}$→dLS projection led to rescuing the preference for social novelty of CSDS-treated mice; however, there were no significant changes in sociability (Fig. 4, C to H). This manipulation also enhanced the approach speed and reduced the avoidance speed when targeting an unfamiliar C57 mouse or unfamiliar CD1 mouse but not a familiar C57 mouse or novel object in the CSDS group (Fig. 4, I and J, and fig. S7, H and I). Optogenetic activation of dCA3$^{CaMKII\alpha+}$→dLS projection also enhanced social preference for the unfamiliar CD1 mouse in CSDS-treated mice (fig. S7, J to L), without affecting anxiety-related or motor behaviors (fig. S7, M and N). However, this manipulation failed to affect novelty-suppressed feeding and real-time place preference behaviors (fig. S7, O and P), suggesting that activation of dCA3$^{CaMKII\alpha+}$→dLS projection increases the preference for social novelty, which is not attributed to the alteration in natural reward-related behaviors. Together, these results indicate that activation of dCA3$^{CaMKII\alpha+}$→dLS projection is necessary for the increase in social novelty preference.

To rule out the possibility that the change in behavior was due to the activation of collateral projections to other brain areas, we used a dual-virus approach to chemogenetically activate dCA3$^{CaMKII\alpha+}$→dLS projection (fig. S8A). Chemogenetic activation of dCA3$^{CaMKII\alpha+}$→dLS projection neurons that express hM3Dq rescued the preference for social novelty of CSDS-treated mice (fig. S8, B to G). This manipulation also enhanced the approach speed and reduced the avoidance speed of CSDS-treated mice when targeting an unfamiliar C57 mouse or an unfamiliar CD1 mouse (fig. S8, H to K). Chemogenetic activation of dCA3$^{CaMKII\alpha+}$→dLS projection neurons also enhanced social preference for the unfamiliar CD1 mouse in the CSDS group (fig. S8, L to N). Collectively, these results indicate that the activity of dCA3$^{CaMKII\alpha+}$→dLS projection neurons regulates the preference for social novelty in mice.

Manipulations of dLS^{GABA+}→PFN projection activity regulate the preference for social novelty in mice

Previous studies have shown that the overwhelming majority of neurons in the dLS are GABAergic neurons and are involved in the regulation of social behaviors (*18*, *28*). We subsequently aimed to investigate whether the dLS^{GABA+}→PFN output circuitry mediates the preference for social novelty in mice. We injected AAV-Vgat-NpHR3.0-EYFP-WPREs-pA into the dLS and found the dense fibers in a defensive-related region, PFN (Fig. 5, A and B, and fig. S9, A and B) (*23*, *24*). To examine whether dLS^{GABA+}→PFN projection was necessary for social novelty preference, we used the dual-virus approach to chemogenetically silence the dLS^{GABA+}→PFN projection neurons during behavior test. Chemogenetic silence of the activity of dLS^{GABA+}→PFN projection neurons also reduced the preference for social novelty in both control and SSDS groups (fig. S10, A to N).

To rule out the possibility that our observed results were due to the inhibition of collateral projections to other brain areas, we optogenetically suppressed the activity of dLS^{GABA+} projection terminals in PFN that express NpHR3.0 by illuminating a continuous yellow laser beam (589 nm, 10 mW) over the PFN during behavior testing. This manipulation reduced the preference for social novelty in both control and SSDS-treated mice; however, there were no significant changes in sociability (Fig. 5, C to H). Optogenetic inhibition of dLS^{GABA+}→PFN projection also reduced the approach speed and enhanced the avoidance speed when targeting an unfamiliar C57 mouse or unfamiliar CD1 mouse but not a familiar C57 mouse or a novel object in both control and SSDS groups (Fig. 5, I and J, and fig. S11, A and B). We also found that optogenetic inhibition of dLS^{GABA+}→PFN projection reduced preference for the unfamiliar CD1 mouse in the SSDS group (fig. S11, C to E), without effect on anxiety-related or motor behaviors (fig. S11, F and G).

To examine whether increased activity of dLS^{GABA+}→PFN projection was sufficient to rescue the preference for social novelty of CSDS-treated mice, we also optogenetically activated the dLS^{GABA+} projection in the PFN that virally expresses ChR2 under the Vgat promoter by illuminating a blue laser beam (20 Hz, 5-ms pulse, 10 mW) over the PFN during behavior testing (Fig. 6, A and B). Optogenetic activation of dLS^{GABA+}→PFN projection rescued the preference for social novelty but not sociability in CSDS-treated mice (Fig. 6, C to H). This manipulation also enhanced the approach speed and reduced the avoidance speed when targeting an unfamiliar C57 mouse or unfamiliar CD1 mouse but not a familiar C57 mouse or novel object in the CSDS group (Fig. 6, I and J, and fig. S11, H and I). We also found that optogenetic activation of dLS^{GABA+}→PFN projection rescued social preference for the unfamiliar CD1 mouse in CSDS-treated mice (fig. S11, J to L), without effect on anxiety-related or motor behaviors (fig. S11, M and N). Furthermore, microinjection of $GABA_A$ receptor blocker (+)-bicuculline (2 μg/ml) in PFN blocked the increase in approach speed and decrease in avoidance speed induced by optogenetic activation of LS^{GABA+}→PFN projection in CSDS-treated mice (fig. S11, O to Q). These results indicate that manipulations of dLS^{GABA+}→PFN projection activity regulate the preference for social novelty of mice.

To rule out the possible influence of the activation of collateral projections of dLS^{GABA+} neurons, we also used the dual-virus approach to chemogenetically activate the dLS^{GABA+}→PFN projection neurons during behavior test. Similar to the results of the optogenetic experiment, chemogenetic activation of the dLS^{GABA+}→PFN projection neurons also rescued the preference for social novelty (fig. S12, A to N). These results further confirmed that the dLS^{GABA+}→PFN projection, as a downstream circuit of dCA3$^{CaMKII\alpha+}$→dLS projection, also regulates the preference for social novelty in mice.

PFN^{Foxb1+} projecting to the lPAG produces social avoidance behavior of mice

Previous studies have indicated that the PFN^{Foxb1+} neurons project to the lateral periaqueductal gray (lPAG) (*24*), which appears to be involved in motivated behavior controlling aversive and more complex motivational processes, such as approach-avoidance conflict resolution (*29*). To construct AAVs that expressed specifically in Foxb1$^+$ neurons, we analyzed the regulatory sequences of Foxb1 reported by another laboratory (*30*) with their possible long-distance enhancers. We next constructed AAV-carrying Cre under the control of a Foxb1-driven promoter and verified their specificity by immunofluorescent colocalization (fig. S13A). We injected the AAV-DIO-ChR2-mCherry combined with AAV-Foxb1-Cre into the PFN to express ChR2 in Foxb1$^+$ neurons (Fig. 7, A and B). Optogenetic activation (20 Hz, 5-ms pulse, 10 mW) of PFN^{Foxb1+}→lPAG projection reduced the preference for a familiar C57 mouse versus a novel object in control mice (Fig. 7C). However, in the social novelty task, optogenetic activation of PFN^{Foxb1+}→lPAG projection failed to change preference for an unfamiliar C57 mouse versus a familiar C57 mouse in the control group (Fig. 7D).

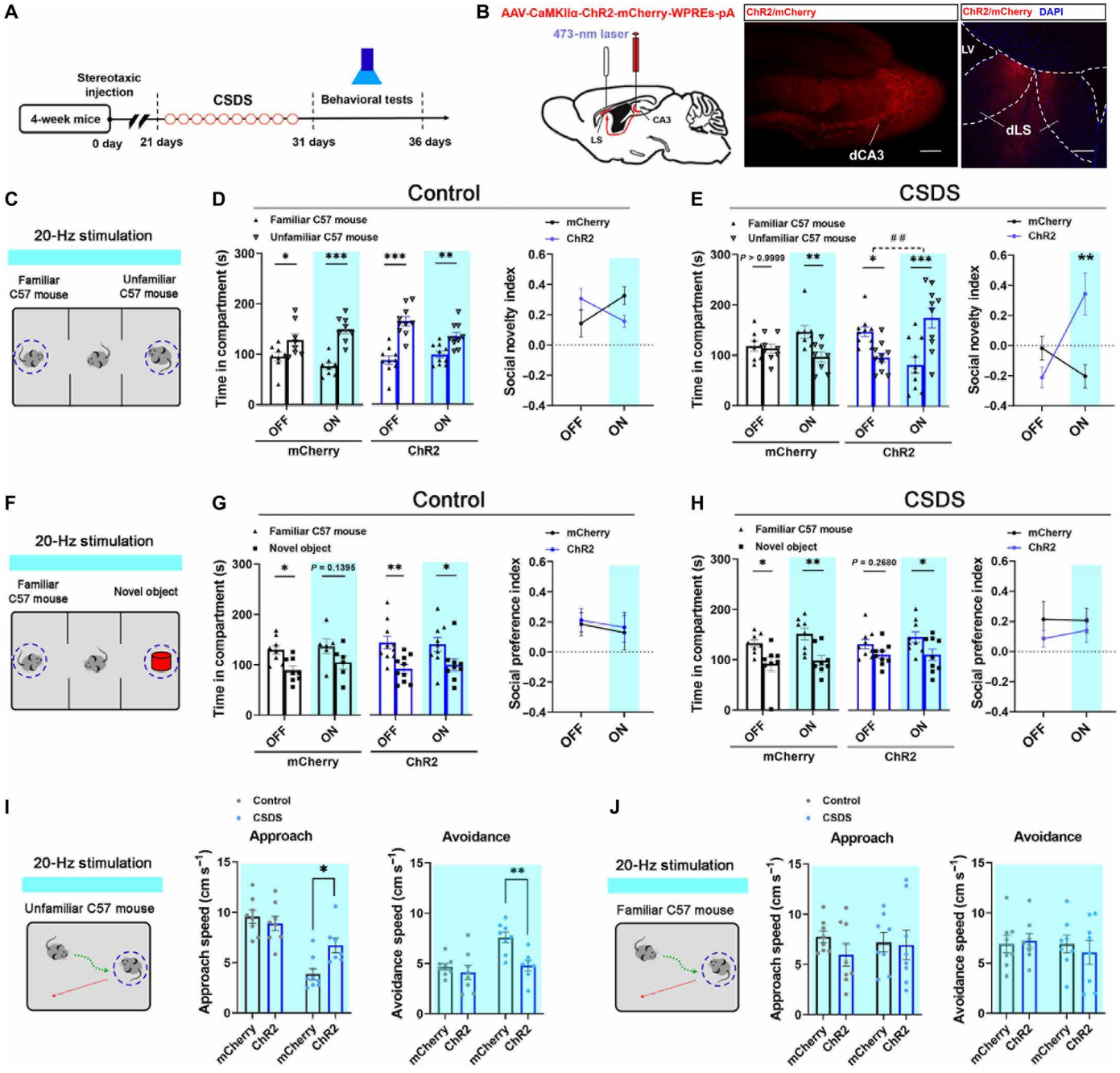

Fig. 4. Optogenetic activation of dCA3$^{CaMKII\alpha+}$→dLS projection rescues the preference for social novelty in CSDS-treated mice. (**A**) Schematic experimental timeline and the behavior test used in optical stimulation experiments. (**B**) Left: Mice were injected into the dCA3 region with AAV and implanted above the dLS with optical fibers. Right: Representative immunofluorescence images of dCA3$^{CaMKII\alpha+}$ neurons and the expression of ChR2-mCherry in dLS terminals. Scale bars, 250 μm (dCA3) and 100 μm (dLS). (**C**) Schematic diagram of optogenetic activation during the three-chamber test with a familiar C57 mouse versus an unfamiliar C57 mouse. (**D** and **E**) Optogenetic activation of dCA3$^{CaMKII\alpha+}$→dLS projection increased the time spent in the compartment with an unfamiliar C57 mouse and social novelty index in CSDS-treated mice (E) but not in control mice (D). Repeated-measures two-way ANOVA followed by Bonferroni's comparisons test, with asterisks depicting familiar C57 mouse versus unfamiliar C57 mouse comparisons, and the dashed line depicting comparisons between OFF and ON in the ChR2 condition. (**F**) Schematic diagram of optogenetic activation during the three-chamber test with a familiar C57 mouse versus a novel object. (**G** and **H**) Optogenetic activation of dCA3$^{CaMKII\alpha+}$→dLS projection produced no change in the time spent in the compartment with a familiar C57 mouse and social preference index in both control (G) and CSDS-treated (H) mice. (**I**) Left: Schematic diagram of optogenetic activation during the approach-avoidance speed test with an unfamiliar C57 mouse. Right: Optogenetic activation of dCA3$^{CaMKII\alpha+}$→dLS projection enhanced the approach speed and decreased the avoidance speed in CSDS-treated mice but not in control mice. (**J**) Left: Schematic diagram of optogenetic activation during the approach-avoidance speed test with a familiar C57 mouse. Right: The approach speed and avoidance speed were unchanged by activation of dCA3$^{CaMKII\alpha+}$→dLS projection in both control and CSDS-treated mice. Data are expressed as means ± SEM. ##$P < 0.01$, *$P < 0.05$, **$P < 0.01$, and ***$P < 0.001$.

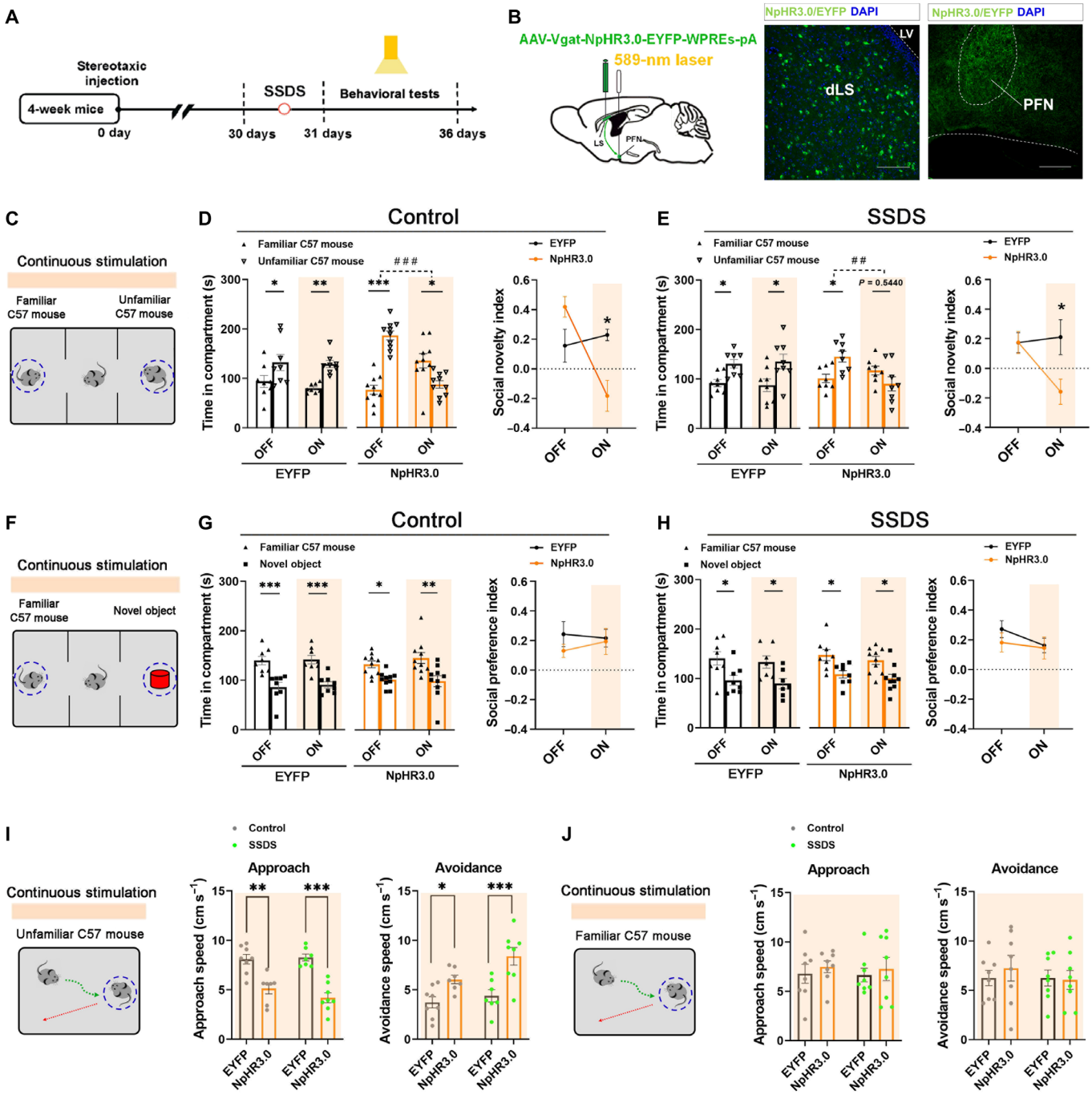

Fig. 5. PFN acts as a downstream target of the dLS^{GABA+} neurons and is involved in the regulation of social novelty preference. (**A**) Schematic experimental timeline of optogenetic inhibition experiments. (**B**) Left: Schematic representation of the virus injection. Mice were injected into the dLS region with AAV and implanted above the PFN with optical fibers. Right: Representative immunofluorescence images of NpHR3.0-EYFP in dLS^{GABA+} neurons and PFN terminals. Scale bars, 50 μm (dLS) and 50 μm (PFN). (**C**) Schematic diagram of optogenetic inhibition during the three-chamber test with a familiar C57 mouse versus an unfamiliar C57 mouse. (**D** and **E**) Optogenetic inhibition of dLS^{GABA+}→PFN projection reduced the time spent in the compartment with an unfamiliar C57 mouse and social novelty index in both control (D) and SSDS-treated (E) mice. Repeated-measures two-way ANOVA followed by Bonferroni's comparisons test, with asterisks depicting familiar C57 mouse versus unfamiliar C57 mouse comparisons, and the dashed line depicting comparisons between OFF and ON in the NpHR3.0 condition. (**F**) Schematic diagram of optogenetic inhibition during the three-chamber test with a familiar C57 mouse versus a novel object. (**G** and **H**) Optogenetic inhibition of dLS^{GABA+}→PFN projection produced no change in the time spent in the compartment with a familiar C57 mouse and social preference index in both control (G) and SSDS-treated (H) mice. (**I**) Left: Schematic diagram of optogenetic inhibition during the approach-avoidance speed test with an unfamiliar C57 mouse. Right: Optogenetic inhibition of dLS^{GABA+}→PFN projection reduced the approach speed in both control and SSDS-treated mice and increased the avoidance speed in SSDS-treated mice. (**J**) Left: Schematic diagram of optogenetic inhibition during the approach-avoidance speed test with a familiar C57 mouse. Right: The approach speed and avoidance speed were unchanged by inhibition of dLS^{GABA+}→PFN projection in both control and SSDS-treated mice. Data are expressed as means ± SEM. ##$P < 0.01$, ###$P < 0.001$, *$P < 0.05$, **$P < 0.01$, and ***$P < 0.001$.

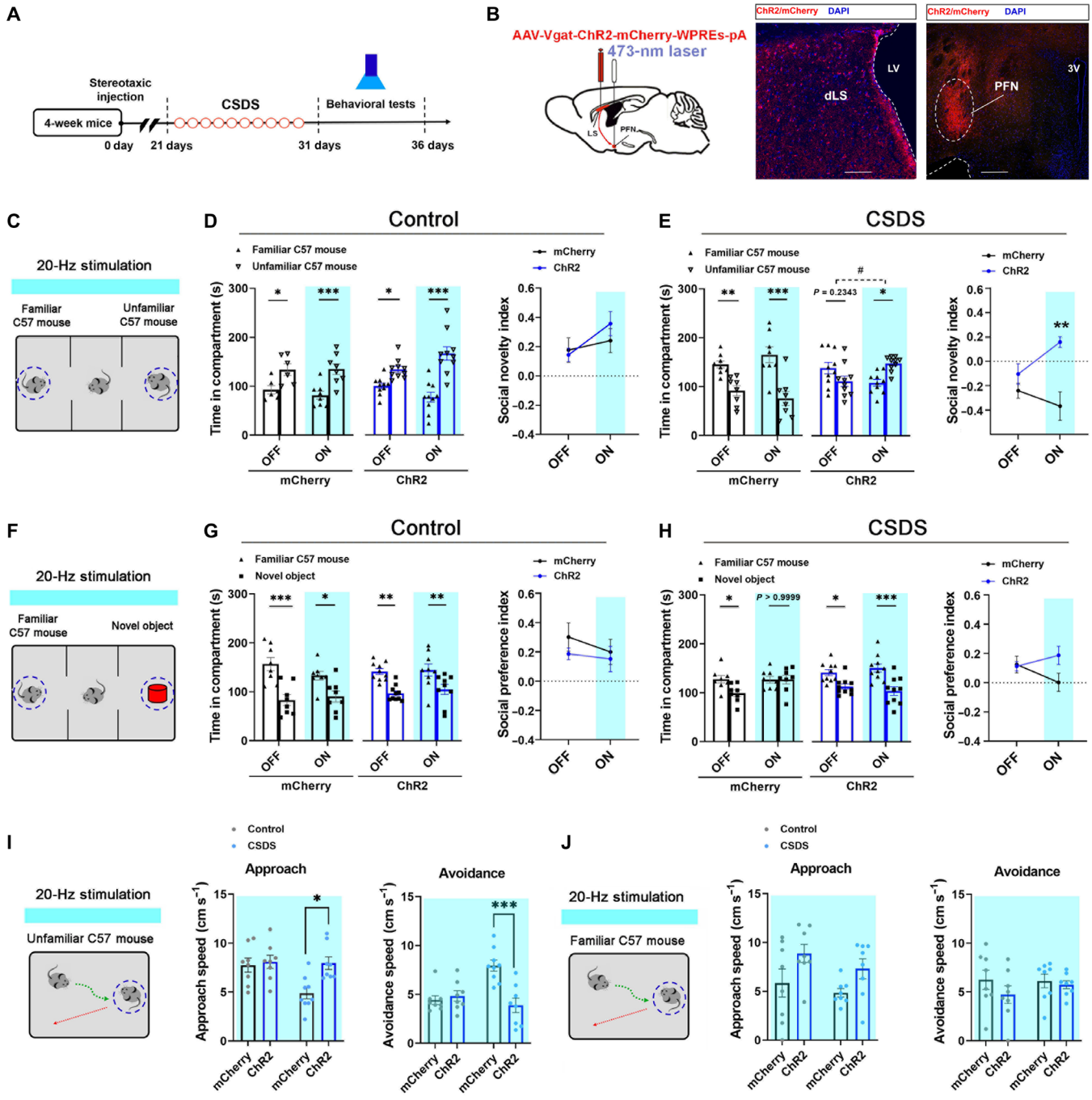

Fig. 6. Optogenetic activation of dLS^{GABA+}→PFN projection rescues the preference for social novelty in CSDS-treated mice. (**A**) Schematic experimental timeline of optogenetic activation experiments. (**B**) Left: Mice were injected into the dLS region with AAV and implanted above the PFN with optical fibers. Right: Representative immunofluorescence images of dLS^{GABA+} neurons and the expression of ChR2-mCherry in PFN terminals. Scale bars, 50 μm (LS) and 50 μm (PFN). (**C**) Schematic diagram of optogenetic activation during the three-chamber test with a familiar C57 mouse versus an unfamiliar C57 mouse. (**D** and **E**) Optogenetic activation of dLS^{GABA+}→PFN projection increased the time spent in the compartment with an unfamiliar C57 mouse and social novelty index in CSDS-treated mice (E) but not in control mice (D). Repeated-measures two-way ANOVA followed by Bonferroni's comparisons test, with asterisks depicting familiar C57 mouse versus unfamiliar C57 mouse comparisons, and the dashed line depicting comparisons between OFF and ON in the ChR2 condition. (**F**) Schematic diagram of optogenetic activation during the three-chamber test with a familiar C57 mouse versus a novel object. (**G** and **H**) Optogenetic activation of dLS^{GABA+}→PFN projection produced no change in the time spent in the compartment with a familiar C57 mouse and social preference index in both control (G) and CSDS-treated (H) mice. (**I**) Left: Schematic diagram of optogenetic activation during the approach-avoidance speed test with an unfamiliar C57 mouse. Right: Optogenetic activation of dLS^{GABA+}→PFN projection enhanced the approach speed and decreased the avoidance speed in CSDS-treated mice but not in control mice. (**J**) Left: Schematic diagram of optogenetic activation during the approach-avoidance speed test with a familiar C57 mouse. Right: The approach speed and avoidance speed were unchanged by activation of dLS^{GABA+}→PFN projection in both control and CSDS-treated mice. Data are expressed as means ± SEM. #$P < 0.05$, *$P < 0.05$, **$P < 0.01$, and ***$P < 0.001$.

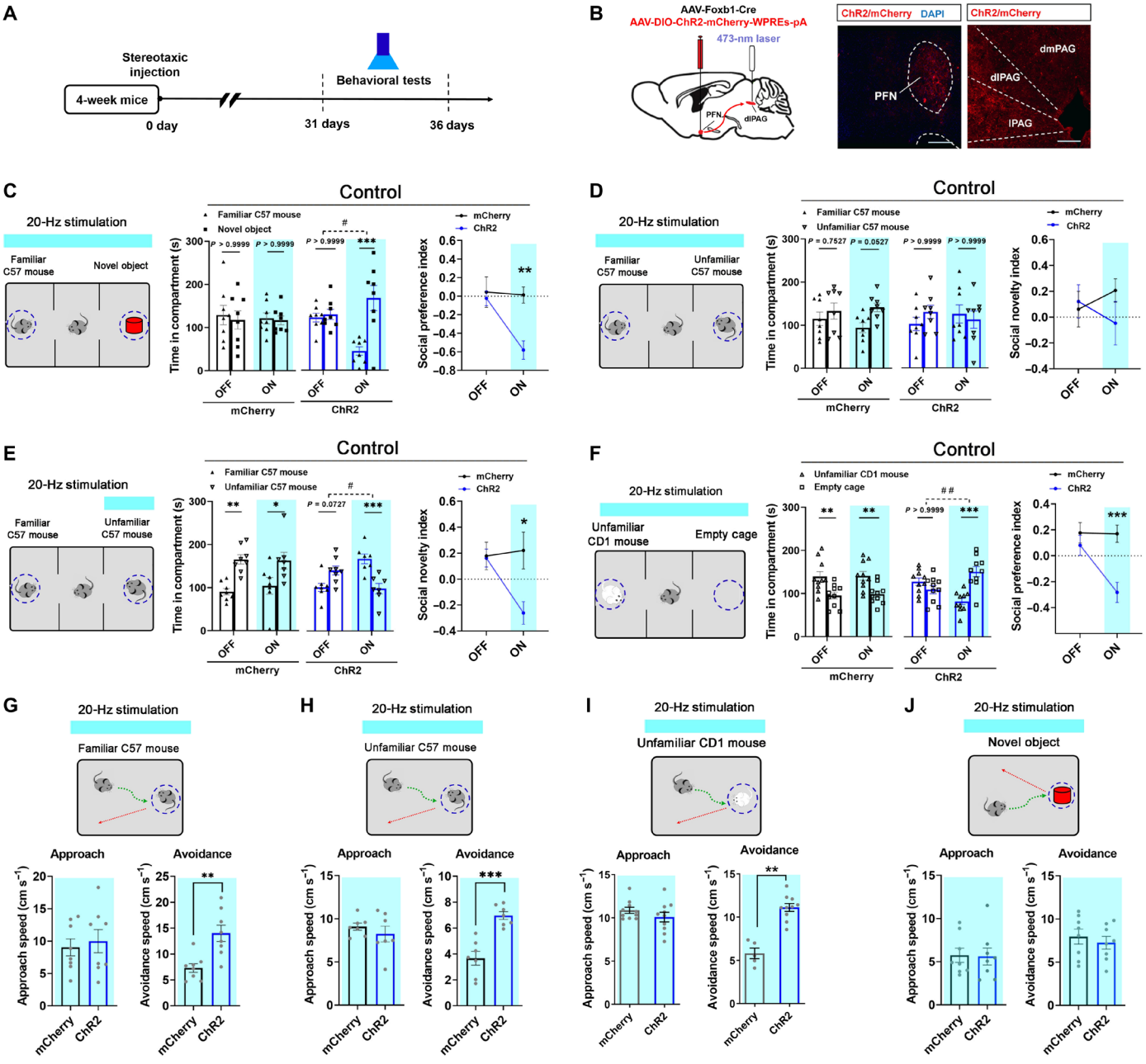

Fig. 7. Optogenetic activation of PFN^{Foxb1+}→lPAG projection induces social avoidance behavior. (**A**) Schematic illustration of the experimental timeline. (**B**) Left: AAV-DIO-ChR2-mCherry-WPREs-pA and AAV-Foxb1-Cre viruses were bilaterally injected into PFN. Right: Representative immunofluorescence images of PFN^{Foxb1+} neurons and the terminals in lPAG expression of ChR2-mCherry. Scale bars, 50 μm. (**C**) Optogenetic activation of PFN^{Foxb1+}→lPAG projection reduced the time spent in the compartment with a familiar C57 mouse and social preference index of control mice during the three-chamber test with a familiar C57 mouse versus a novel object. (**D**) Optogenetic activation of PFN^{Foxb1+}→lPAG projection produced no effect on social novelty index of control mice during the three-chamber test with a familiar C57 mouse versus an unfamiliar C57 mouse. (**E**) Optogenetic activation of dCA3$^{CaMKII\alpha+}$→dLS projection within the unfamiliar C57 mouse chamber reduced the time spent in the compartment with an unfamiliar C57 mouse and social novelty index of control mice during the three-chamber test with a familiar C57 mouse versus an unfamiliar C57 mouse. (**F**) Optogenetic activation of PFN^{Foxb1+}→lPAG projection reduced the time spent in the compartment with an unfamiliar CD1 mouse and social preference index of control mice during the three-chamber test with an unfamiliar CD1 mouse versus an empty cage. (**G** to **I**) Optogenetic activation of PFN^{Foxb1+}→lPAG projection produced no difference in approach speed but promoted social avoidance speed with a familiar C57 mouse (G), an unfamiliar C57 mouse (H), and an unfamiliar CD1 mouse (I) in the control group. (**J**) Optogenetic activation of PFN^{Foxb1+}→lPAG projection produced no difference in approach and avoidance speed with a novel object in the control group. Data are expressed as means ± SEM. #$P < 0.05$, ##$P < 0.01$, *$P < 0.05$, **$P < 0.01$, and ***$P < 0.001$. dmPAG, dorsomedial periaqueductal gray; dlPAG, dorsolateral periaqueductal gray.

To examine whether PFN^{Foxb1+}→lPAG projection activity is sufficient to decrease the preference for social novelty in mice, we optogenetically activated PFN^{Foxb1+}→lPAG projection within the unfamiliar C57 mouse chamber. This manipulation reduced the preference for social novelty in control mice (Fig. 7E). Optogenetic activation of PFN^{Foxb1+}→lPAG projection also reduced social interaction time with the unfamiliar CD1 mouse in the control group (Fig. 7F). Optogenetic activation of PFN^{Foxb1+}→lPAG projection also significantly enhanced the avoidance speed when targeting a familiar C57 mouse, unfamiliar CD1 mouse, and unfamiliar C57 mouse but not a novel object in the control group. However, there were no significant changes in approach speed (Fig. 7, G to J). Optogenetic activation of PFN^{Foxb1+}→lPAG projection directly induced avoidance behavior of control mice during social approach (movie S1). These results suggest that the PFN^{Foxb1+}→lPAG projection mediates the avoidance of general social situations. However, optogenetic inhibition of PFN^{Foxb1+}→lPAG projection produced no noticeable change in social behaviors of control mice (fig. S13, B to I). Neither optogenetic activation nor silence of PFN^{Foxb1+} axons affected the behavior in OFT and TST (fig. S13, J to M). Collectively, these results demonstrate that PFN^{Foxb1+}→lPAG projection produces avoidance behaviors of general social situations.

Dissection of the dCA3$^{CaMKII\alpha+}$→dLS^{GABA+}→PFN^{Foxb1+} circuit

To characterize the connectivity of the dCA3$^{CaMKII\alpha+}$→dLS^{GABA+}→PFN^{Foxb1+} circuit, we took advantage of a combinatorial strategy that permits direct visualization of these projections (fig. S14A). We initially injected a retrogradely transported retroAAV (AAV2/2Retro-hSyn-Cre-EGFP) into the PFN that allowed the virus to spread retrogradely into the soma of dLS neurons to express Cre-GFP (green fluorescent protein). The Cre-dependent retrograde transmonosynaptic tracing system (AAV-DIO-RVG, AAV-DIO-TVA-GFP, and RV-EvnA-ΔG-DsRed) was subsequently used to express the Cre enzyme in dLS neurons. It was shown that there were numerous DsRed^{+} cell bodies in the pyramidal layer of dCA3 (fig. S14B). We also used cholera toxin B subunit (CTB) for retrograde tracing of the projections. In dLS, we found that the retrograde CTB from PFN was colocalized with Vgat (fig. S14, C to E). To assess the functional synaptic connectivity of the circuit, we recorded the optogenetic excitatory postsynaptic currents (oEPSCs) in dLS neurons and the optogenetic inhibitory postsynaptic currents (oIPSCs) in PFN^{Foxb1+} neurons (fig. S14, F and G). Together, these results identify long-range dCA3$^{CaMKII\alpha+}$→dLS^{GABA+}→PFN^{Foxb1+} circuits.

To gain insight into whether dCA3 controlled the preference for social novelty through regulating the PFN^{Foxb1+}→lPAG projection, we injected pseudorabies virus 152 (PRV-152) directly into the lPAG of mice to retrogradely and transsynaptically label the upstream neurons (*31*). PRV-152 is a transsynaptic retrograde herpes virus driving expression of GFP, which is often used as a tracer for mapping neural circuits (*32*). The mice were euthanized at different time points after PRV-152 injection to unravel in which order the virus went back anterogradely, and the fluorescence intensities were measured at different time points in the PFN, dLS, and dCA3, respectively (fig. S15A), indicating that a subset of dCA3 neurons has indirect projections to the lPAG by passing through the dLS and PFN sequentially. We also observed the expression of immediate early gene c-Fos in dCA3, dLS, PFN, and lPAG after exposure to an unfamiliar C57 mouse in control and CSDS groups. c-Fos fluorescence was highly expressed in dCA3 and dLS of control mice and highly expressed in PFN and lPAG of CSDS-treated mice (fig. S15, B and C). However, we cannot exclude the possibility that the neurons in other brain areas might be activated or inhibited by a social stimulus (an unfamiliar mouse). Collectively, these results indicate that the activity of dCA3$^{CaMKII\alpha+}$→dLS^{GABA+} circuit regulates the preference for social novelty of mice through inhibiting the PFN^{Foxb1+}→lPAG projection.

The changes in the expression of potassium channels are involved in the reduced excitability of dCA3 neurons induced by exposure to social defeats

Next, we sought to understand the molecular adaptation induced by CSDS in dCA3 by the use of RNA sequencing (RNA-seq) from control and CSDS-treated mice. For differential expression analysis, we removed transcripts with less than 1000 to identify differentially expressed transcripts (DETs) from paired RNA-seq data in dCA3 neurons in response to CSDS exposure. We found that 148 transcripts were up-regulated and 103 transcripts were down-regulated by CSDS (Fig. 8A).

The database for annotation, visualization, and integrated discovery (DAVID) was used to obtain the functional gene ontology (GO) of the 251 DETs in dCA3 neurons to determine the specific target of transcriptional alteration in dCA3 induced by CSDS. We found that 10 cellular subcompartments were significantly enriched in our DET dataset, which contributed to neuronal excitability (Fig. 8B). On the basis of these results, we further investigated the changes in the expression of K^{+} channels in dCA3 (Fig. 8, C and D). There was obvious up-regulation in Kir2.4 (*Kcnj14*) in the defeated mice. Previous studies have demonstrated that the up-regulation of Kir2.4, an integral membrane protein and inward-rectifier potassium channel, reduced intrinsic excitability of neurons (*33*). The above results indicate that CSDS suppresses the excitability of dCA3 neurons by regulating the expression of Kir2.4.

DISCUSSION

Here, we reported that the excitability of dCA3$^{CaMKII\alpha+}$ neurons, which play a critical role in the preference of social novelty, was particularly enhanced when an animal explored an unfamiliar conspecific. At the population level, inhibition of dCA3$^{CaMKII\alpha+}$ neurons led to the avoidance of an unfamiliar mouse and reduction of social novelty preference. The preference for social novelty is necessary for the social life of animals, which is vulnerable to social stress. We found that exposure to social defeat stress induced the deficits of social novelty in mice by impairing the responses of dCA3$^{CaMKII\alpha+}$ neurons when targeting an unfamiliar mouse. By using viral tracing and optogenetic and chemogenetic manipulations, we demonstrated that the dCA3$^{CaMKII\alpha+}$→dLS^{GABA+}→PFN^{Foxb1+}→lPAG circuit controlled the preference of social novelty in mice (Fig. 8E).

In the classic pathway, social information proceeds from the EC to DG to CA3 and next to CA1, the main hippocampal output (*34*). Social recognition memory is crucial for survival across species, underlying the need to correctly identify social novelty (*7*). Furthermore, in hippocampus, there is a clear functional distinction along the dorsal/ventral axis in regulating social memory. Silencing dCA1 does not disrupt social recognition memory; however, identical manipulations in vCA1 impair the behavior (*35*). Chiang *et al.* (*6*) reported that vCA3 function is required for the encoding. However,

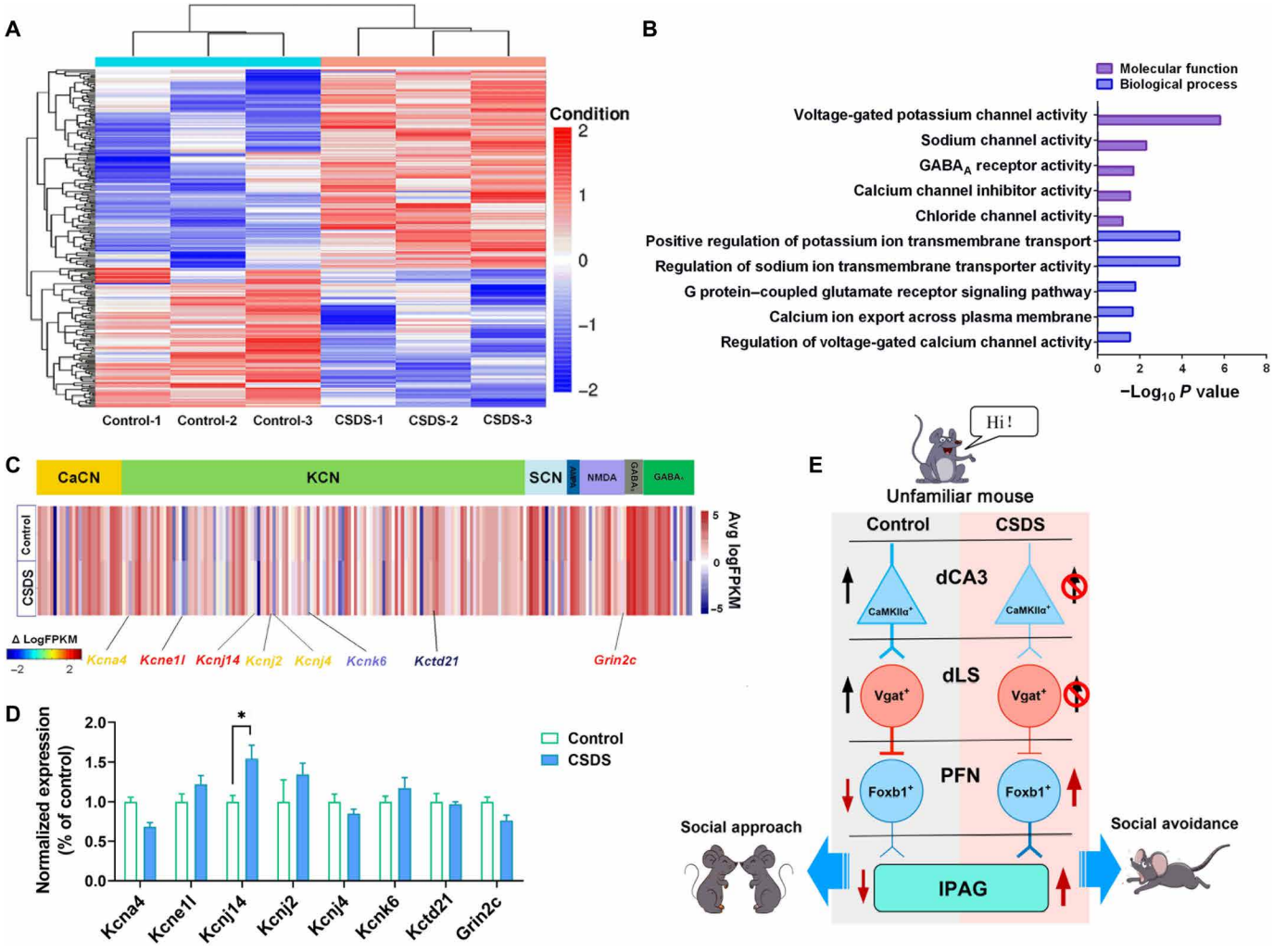

Fig. 8. CSDS decreases the excitability of dCA3$^{CaMKII\alpha+}$ neurons by influencing the expression of K$^+$ channels. (**A**) FPKM heatmaps of 245 DEGs in the dCA3 region between control and defeated mice as ranked by differential expression LimmaVoom log ratio ($log_2FC > 0.58$, $P < 0.05$). (**B**) DETs were enriched for GO terms related to multiple neuronal compartments (Bonferroni test, $P < 0.05$), especially for the genes that regulate neuronal excitability. (**C**) The expression profiling of neuronal ion channels in the dCA3 region. Average expression of each transcript is shown as a vertical line for each treatment group. Blue transcripts are lower expression, whereas red transcripts are higher expression. The significant alterations in the transcription of specific channels induced by chronic stress are depicted by the font color of the gene name, in which red represents the increased expression, and blue indicates the decreased expression. NMDA, *N*-methyl-D-aspartate. (**D**) The changes in expression of the K$^+$ channel and receptor genes in response to CSDS in the dCA3 region. (**E**) Summary of the circuits from dCA3 to lPAG. The dCA3$^{CaMKII\alpha+}$ neurons were activated by stimulation of unfamiliar mice from either conspecifics or contraspecifics and promoted social novelty signals through its output to dLS^{GABA+} neurons, which inhibited the PFN^{Foxb1+}→lPAG circuits and enhanced the preference for social novelty. CSDS impaired the response of dCA3$^{CaMKII\alpha+}$ neurons to unfamiliar mice, which led to a disinhibition of dLS^{GABA+}→PFN^{Foxb1+} circuits and enhanced the activity of lPAG, and eventually caused the deficits of social novelty preference. Data are expressed as means ± SEM. *$P < 0.05$.

these studies focus on the encoding but not the identification for an unfamiliar mouse. In our study, dCA3$^{CaMKII\alpha+}$ neurons were activated during the identification for an unfamiliar mouse and induced the preference for social novelty, indicating that dCA3 is directly involved in the regulation of social recognition. The CaMKIIα is also expressed in CA2 pyramidal neurons, and recent work has demonstrated that the CA2 region encodes social recognition memory (*7*). Our results not only represent an important addition to the existing neural networks of social recognition memory but also further clarify a larger social circuit across the multiple axes of the hippocampus.

When receiving the social novelty information, dCA3 translates signals through its strong projection to dLS, and LS plays an important role in social approach (*36*). Oxytocin receptors were enriched in LS and specifically regulated social behavior (*37*, *38*). These oxytocin receptor–positive neurons in LS may be involved in the preference of social novelty. Leroy *et al.* (*39*) reported a microcircuit within the LS where projections from the dLS to the vLS directly drove social behaviors. This circuit promotes aggressive behavior by connecting dCA2 and the ventrolateral part of the ventromedial hypothalamus. CA2 inputs to CA3 also participate in the deficit of preference for social novelty (*40*, *41*). In our study, the tracing retrograde results showed that the neurons projecting to PFN were mainly located in the dLS and only very few in the vLS. These two circuits play different roles in the regulation of behavior, in which the dLS→PFN projection regulates the preference for social novelty. However, our results cannot exclude the possible role

of the vLS→PFN circuit in social behavior. Our neural circuit retrograde tracing results suggest that the dCA3$^{CaMKII\alpha+}$→dLS^{GABA+}→PFN^{Foxb1+} circuit is a separate circuit. Furthermore, in terms of structure and function, dCA2→dLS and dCA3→dLS may be two separate and parallel circuits from the dorsal hippocampus; however, the bifurcation of social behaviors might occur at the level of dLS but not at the level of the hippocampus. Our findings provide new information for the neural network relevant to the regulation of social behavior.

Here, we described the ability of PFN^{Foxb1+} neurons to control avoidance behavior. The PFN is located in the ventrolateral hypothalamus (*23*). In our study, we found that the strong activity of dCA3$^{CaMKII\alpha+}$→dLS^{GABA+} projection produced signals to suppress PFN^{Foxb1+} neuronal activity and enhanced social approach behavior. Conversely, silencing the circuit disinhibited PFN^{Foxb1+} neurons and caused social avoidance behavior. By using pharmacological methods, we found that the $GABA_A$ receptors of PFN were the potential target for treatment of social avoidance. Future studies are needed to explore the physiological function of PFN^{Foxb1+} neurons.

Animal research has a long history of relying on paradigms related to approach-avoidance balance to model social behavior (*42*). Lange and Pauli (*43*) assessed the motivation level of mice in social interaction behavior by measuring their approach-avoidance speed. The drive to approach and to explore novel conspecifics is inherent to social animals and may promote optimal social functioning. Since novelty exploration often engages in risky behaviors, approaching novel stimuli may require not only the motivation to approach and explore but also the suppression of risk avoidance (*44*). Therefore, there are two possible frameworks for how approach-avoidance balance regulates the preference for social novelty. Framework 1 supposes a hedonic approach to social novelty. When exposed to an unfamiliar mouse, the hedonic and/or motivational value of social novelty is enhanced to overcome the risk avoidance, leading to the preference for social novelty (*45*). Framework 2 supposes an inherent avoidance for risk. Under a state of anxiety or social fear, inherent risk avoidance is enhanced, leading to the avoidance of social novelty (*46*). On the basis of the present results, the dCA3$^{CaMKII\alpha+}$→dLS^{GABA+}→PFN^{Foxb1+} circuit was in accordance with framework 1, in which activation of the circuit increased the speed of approach while decreasing the speed of avoidance in CSDS-treated mice, enhancing the preference for social novelty, while the action of the PFN^{Foxb1+}→lPAG circuit was in accordance with framework 2, in which activation of the circuit increased avoidance speed, but inhibition of this circuit had little impact on the social approach behavior directly. However, there are several limitations of these frameworks. First, the speed does not fully represent the intrinsic motivation of animals. Second, the change in approach speed did not correspond to the change in avoidance speed. These frameworks need to be further studied in the future.

Our study found that activation of the dCA3$^{CaMKII\alpha+}$→dLS circuit did not show obvious effects in control mice, which may result from their high baseline activity of dCA3$^{CaMKII\alpha+}$ neurons. SSDS was used to examine whether the circuit was involved in the regulation of susceptibility of mice to social stress. We also found that the circuit regulated the social preference for an unfamiliar CD1 mouse, which was in line with similar findings reported earlier (*47*). Our results also indicate that CSDS reduced the neuronal excitability of dCA3 by altering the expression of potassium channels. However, further research is needed to investigate the role of Kir2.4 in social behaviors.

In humans, there is strong evidence to indicate that social stress can result in deficits of social novelty preference (*48*). We found that dCA3$^{CaMKII\alpha+}$ neurons specifically were activated during social novelty preference. Our results indicated that the preference for social novelty was regulated by an independent yet connected circuit of dCA3$^{CaMKII\alpha+}$→dLS^{GABA+}→PFN^{Foxb1+}→lPAG. The current results provide insight into how dCA3 dysfunction might contribute to the deficits in the preference for social novelty, providing new information for the potential therapeutic targets for neuropsychiatric diseases.

MATERIALS AND METHODS

Animals

Adult male C57BL/6J (C57) mice (4 to 5 weeks old) were purchased from Hunan SJA Laboratory Animal Co. Ltd. (Changsha, Hunan, China). Mice were bred and maintained in the Animal Resource Centre of Tongji Medical College, Huazhong University of Science and Technology. The C57BL/6J mice were housed in groups of four or five per cage in plastic cages and maintained under standard laboratory conditions (12-hour light/12-hour dark cycle at a constant temperature of 22° ± 2°C with free access to food and water) unless otherwise indicated. All animal procedures were conducted in accordance with the National Institutes of Health *Guide for the Care and Use of Laboratory Animals* and approved by the Animal Welfare Committee of Huazhong University of Science and Technology.

Method details

Stereotaxic surgery

Mice were anesthetized with 1 to 2% isoflurane in oxygen and placed in a stereotaxic frame (RWD510, RWD Technology, Shenzhen, China) with a heated pad underneath. Animals were kept at a stable depth of anesthesia, characterized by a loss of reflexes and a respiration rate of 100 to 120 breaths/min. A scalp incision was made with eye scissors. A craniotomy (0.5 mm × 0.5 mm) was made with a dental drill.

For microinjection of virus. The AAVs in table S1 were used for optical fiber–based Ca^{2+} recordings and optogenetic and chemogenetic experiments. All AAVs were purchased from BrainVTA Technology (Wuhan, China). PRV-152 was used as a retrograde and transsynaptic label from BrainVTA Technology Co. A volume of 50 to 100 nl of AAV solution was injected at each site. After each injection, the micropipette was held in place for 5 to 10 min before being slowly retracted. The injection coordinates were based on the *Paxios and Franklin Mouse Brain Atlas*, second edition. The coordinates were as follows: for dCA3: anteroposterior (AP), −1.90 mm; mediolateral (ML), ±2.00 mm; Dorsoventral (DV), −2.10 mm; for LS: AP, +0.59 mm; ML, ±0.35 mm; DV, −2.55 mm; for PFN: AP, −1.50 mm; ML, ±1.25 mm; DV, −5.20 mm; and for lPAG: AP, −4.35 mm; ML, ±0.55 mm; DV, −2.25 mm. Depending on the spread of the reagent injected, one injection site was made at the AP axis per side to achieve sufficient coverage of the desired region. Following injections, the scalp incision was closed using surgical sutures. Mice were returned to their home cages and allowed to recover for about 3 weeks before Ca^{2+} recordings and other behavioral tests. CTB-488 (c34775, Invitrogen, Waltham, USA) was injected through a small glass micropipette with a tip diameter of 10 μm for 5 min. The micropipette was held in place for 5 to 10 min before retraction to retrograde neurons in dCA3.

For implantation of optical fibers and cannulas. Briefly, to optically stimulate terminals, optic fibers were bilaterally implanted into the LS (AP, +0.59 mm; ML, ±0.35 mm; DV, −2.55 mm), PFN (AP, −1.50 mm; ML, ±1.25 mm; DV, −5.20 mm), and lPAG (AP, −4.35 mm; ML, ±0.55 mm; DV, −2.25 mm). For fiber photometry, the optical fiber was implanted into the dCA3 (AP, −1.90 mm; ML, ±2.00 mm; DV, −2.10 mm). For pharmacological experiments, drug cannulas were bilaterally implanted into the PFN (AP, −1.50 mm; ML, ±1.25 mm; DV, −5.20 mm). Mice had at least 1 to 2 weeks to recover after surgery.

Fiber photometry

Optical fiber–based Ca^{2+} recordings were performed using a custom-built setup (FiberOptoMeter, Thinker Tech Co., Nanjing, China). An optical fiber (200 μm in diameter, numerical aperture of 0.39, FT200UMT, NEWDOOM, Hangzhou, China) was slowly inserted into dCA3. The fiber tip was typically advanced to a depth of 1.80 mm. Light intensity at the tip of the fiber was 0.20 mW/mm^2. GCaMP6m mice were implanted with an optic fiber 3 weeks after AAV injection and were allowed to recover for 5 to 7 days afterward before behavioral testing. Neuronal Ca^{2+} signals and behavior videos were recorded simultaneously. Ca^{2+} signals were sampled at 2000 Hz through customized acquisition software (Thinker Tech Co., Nanjing, China). GCaMP6m mice were placed in a cage (30 cm by 15 cm) and exposed to social interaction with an empty cage, a novel object, a familiar C57 mouse, and an unfamiliar C57 mouse in turn (diameter, 8 cm). GCaMP6m-treated mice were also placed in the cage and exposed to social interaction with a familiar CD1 mouse and an unfamiliar CD1 mouse in the next day. During the test, the neuronal activity and behavioral responses of mice were synchronously recorded. Behavioral videos were recorded at 30 Hz using a video camera (CS-H100, AniLab Co., Ningbo, China). All fiber photometry data and behavior videos were aligned offline through event markers.

Histology, immunohistochemistry, and microscopy

Mice received an overdose of chloral hydrate [10% (w/v), 300 mg/kg of body weight, i.p.] and were then transcardially perfused with cold phosphate-buffered saline (PBS), followed by ice-cold 4% paraformaldehyde (PFA; Sigma-Aldrich) in PBS. Brains were removed and submerged in 4% PFA at 4°C overnight to postfix and then transferred to 30% sucrose to equilibrate. Coronal brain sections (40 μm) were obtained on a cryostat microtome (Leica CM1950, Germany). Freely floating sections were washed with PBS and blocking solution [0.3% Triton X-100 and 10% normal goat serum (NGS) in PBS] for 1 hour at room temperature. Sections were then incubated in primary antiserum [anti–c-Fos, 1:1000 (Abcam); anti-CaMKIIα, 1:100 (Millipore); anti-Vgat, 1:200 (Abcam); anti-Foxb1, 1:200 (Abcam); details of antibodies are shown in table S2] diluted in PBS with 3% NGS and 0.1% Triton X-100 overnight. The secondary antibodies used were Alexa Fluor 488, 594, or 405 goat anti-mouse immunoglobulin G and Alexa Fluor 488, 594, or 405 goat anti-rabbit (Jackson ImmunoResearch, West Grove, USA; details of antibodies are shown in key resources of table S2) at room temperature for 1 hour. Sections were mounted and coverslipped with anti-fade reagent with 4′,6-diamidino-2-phenylindole (DAPI; ProLong Gold Antifade Reagent with DAPI, Life Technologies, Waltham, USA). Sections were then photographed and analyzed with an OLYMPUS laser scanning confocal microscope (FV1200, OLYMPUS, Tokyo, Japan).

For c-Fos staining experiment, mice were euthanized 1.5 hours after social interaction stimulus, and brains were then subjected to c-Fos staining. The images were taken and then overlaid with the Mouse Brain in Stereotaxic Coordinates of dCA3 (from bregma: −1.70 to 2.00 mm). Then, the c-Fos staining was manually counted by an individual experimenter blind to the experiment groups.

Electrophysiological recording

The coronal slices (300 μm) from 10- to 12-week-old mice that received virus injections for 6 weeks were prepared. Patch-clamp recording in dCA3 was made on visually identified neurons expressing EYFP. Coronal sections were cut with a vibratome (Leica V1000S) into an ice-cold oxygenated solution containing 110 mM choline chloride, 2.5 mM KCl, 1.3 mM sodium phosphate buffer, 25 mM $NaHCO_3$, 1.3 mM Na-ascorbate, 0.6 mM Na-pyruvate, 0.5 mM $CaCl_2$, and 7 mM $MgCl_2$. Then, slices were incubated at 28°C for 30 min in artificial cerebrospinal fluid (ACSF) containing 125 mM NaCl, 2.5 mM KCl, 1.3 mM sodium phosphate buffer, 25 mM $NaHCO_3$, 1.3 mM Na-ascorbate, 0.6 mM Na-pyruvate, 10 mM glucose, 2 mM $CaCl_2$, and 1.3 mM $MgCl_2$ (pH 7.35 when saturated with 95% O_2/5% CO_2) and allowed to equilibrate to room temperature for >30 min. The osmolarity of all solutions was maintained at 280 to 300 mosM.

Pipettes were formed using a micropipette puller (Sutter P-2000) with a resistance of 3 to 5 megohms. During whole-cell patch-clamp recording, we viewed individual cells with an upright fixed-stage microscope (FN-S2N, Nikon, Tokyo, Japan) equipped with a water immersion objective (40×, 0.8 numerical aperture), infrared-filtered light, differential interference contrast optics, and a Coolsnap HQ charge-coupled device camera (Photometrics, Britannia). All recordings were conducted with a MultiClamp700B amplifier (Molecular Devices, Sunnyvale, USA). Analog signals were low-pass–filtered at 2 kHz, digitized at 20 kHz using Digidata 1440A, and recorded using pClamp 10 software (Molecular Devices, Sunnyvale, USA).

Evoked EPSCs were induced using a 500-ms blue light (5-ms pulse, 20 Hz) stimulation of the LS terminals of $CaMKII\alpha^+$ neurons expressing ChR2 from dCA3 soma projecting to the LS. Recordings were performed on $Vgat^+$ neurons (EYFP positive) with pipettes filled with 105 mM potassium gluconate, 30 mM KCl, 10 mM Hepes, 10 mM phosphocreatine, 0.3 mM EGTA, 5 mM QX314, 4 mM Mg-GTP (guanosine 5′-triphosphate), and 0.3 mM Na-ATP (adenosine 5′-triphosphate) (pH 7.35). To identify the evoked EPSCs, ionotropic glutamate receptor antagonists D-2-amino-5-phosphonovalerate (AP-5; 25 μM) and 2,3-dihydroxy-6-nitro-7-sulfamoyl-benzoquinoxaline-2,3-dione (NBQX; 20 μM) were added at the end of recordings. We also recorded the evoked EPSCs of vlPAG terminals of $Foxb1^+$ neurons expressing ChR2 from PFN soma projecting to the vlPAG with the above method.

Evoked IPSCs were elicited using a 500-ms blue light (5-ms pulse, 60 Hz) stimulation of PFN axon terminals of GABAergic neurons expressing ChR2 from the LS. Recordings were performed on PFN $Foxb1^+$ neurons with pipettes filled with 130 mM cesium gluconate, 7 mM CsCl, 10 mM Hepes, 2 mM $MgCl_2$, 4 mM Mg-ATP, 0.3 mM tris-GTP, and 8 mM QX314 (pH 7.25). To rule out glutamatergic inputs, ionotropic glutamate receptor antagonists AP-5 (25 μM) and NBQX (20 μM) were added to ACSF. To identify the evoked IPSCs, $GABA_A$ receptor antagonist bicuculline (25 μM) was added at the end of recordings. The severity of aggressive attacks of CD1 mice has been screened before the CSDS procedure to maintain the homogeneity of aggression of CD1 mice (*49*).

The excitability of $CaMKII\alpha^+$ neurons was validated within the dCA3 in each recording. Whole-cell patch-clamp recordings were

obtained from dCA3 brain slices (350 μm). Spike number was obtained by 50-pA current injections in 0.5-s increments in current-clamp mode, as a measure of intrinsic neuronal excitability. Whole-cell quantification of current injection–induced first spike numbers was used to determine the rheobase.

Chronic social defeat stress

CSDS was performed as previously reported. A single C57 intruder mouse was exposed to a different CD1 aggressor mouse for 5 to 10 min each day for a total of 10 days. The severity of aggressive attacks of CD1 mice had been screened before the CSDS procedure to maintain the homogeneity of aggression of CD1 mice. Following 5 to 10 min of contact, the intruder C57 mouse was housed across a perforated Plexiglass divider, providing further stressful sensory cues from the aggressor CD1 mouse for the remainder of the 24-hour period. Control C57 mice were pair-housed in defeat boxes with one mouse per side of the perforated divider. All control mice that were placed with the controls were changed daily. On day 11, defeated animals were subjected to the behavior tests.

Subthreshold social defeat stress

Mice were subjected to SSDS as described previously with minor modification (*50*). Briefly, the C57 mouse was placed into the home cage of a CD1 mouse for 3 min during which time the experimental mouse was physically defeated by the CD1 mouse. After 3 min of physical interaction, the experimental mouse underwent 10 min of sensory stress. For this, a plastic divider with holes was placed in the middle of the home cage of the CD1 mouse, and the resident CD1 and intruder experimental mice were physically separated but kept next to each other. After three bouts of defeats, the experimental mouse was returned to its home cage and underwent behavioral test on the next day. SSDS is used to investigate the impact of neural circuits on stress vulnerability behavior. SSDS is a mild stimulus, which is also used as the control group of CSDS. The main difference between SSDS and CSDS is that SSDS mice have social defeat experience, but it does not directly affect behavior.

Behavioral tests

All mice were habituated to each test apparatus for 60 min. All experiments were conducted blind to genotype and treatment group. Randomization was done by the experimenter, and no subject or data were excluded for any reason. For optogenetic experiments, three continuous sessions of tests were conducted (pre-session and opto-session); the laser was turned off in the pre-session and turned on during the opto-session test. For chemical-genetic experiments, three sessions of tests were conducted on two consecutive days, and CNO was injected before the session on the second day. Mouse behavior was video-tracked (ANY-maze), and sniffing time was manually scored with ANY-maze software (ANY-maze v5.3, Stoelting, USA). The detection systems for social behavior tests and optogenetic stimulation are both from AniLab Co. (AES-LOC4, Ningbo, China).

Social interaction test

SIT was composed of two 150-s phases. All data during these phases were automatically recorded by ANY-maze. During the first phase, the C57 mouse was allowed to explore freely in a square-shaped open-field arena (45 cm by 45 cm by 45 cm) having a wire-mesh cage (10 cm by 6 cm) opposed to one side, with their movement tracked in the absence of the aggressor. In the second phase, the mouse was reintroduced into this arena with an unfamiliar CD1 mouse within the cage. After each phase, the apparatus was cleaned with a solution of 70% ethanol in water to remove olfactory cues, and all of the behavioral tests were conducted under red-light conditions in a room isolated from external sound sources. According to the time spent in the interaction zone (14 cm by 26 cm) during the first (no target) and second (target) phase, the ratio of time in the interaction zone during target (in the presence of an unfamiliar CD1 mouse) versus no target (in the absence of CD1 mouse) phase in SIT was measured. Defeated mice were divided into susceptible and resilient groups according to whether they exhibited social avoidance [susceptible, social interaction ratio (SIR) < 1] or social preference (resilient, SIR ≥ 1).

Social approach-avoidance speed test

Social approach-avoidance speed test was composed of three 150-s phases. The real-time speed of mice during these phases was automatically recorded by ANY-maze. The C57 mouse was allowed to explore freely in a square-shaped open-field arena (45 cm by 45 cm by 45 cm) having a wire-mesh cage (10 cm by 6 cm) opposed to one side. An interaction zone (14 cm by 26 cm) was identified around the cage. The position of mice was also marked in real time, and when mice entered the interaction zone, this speed was recorded as social approach speed, and the corresponding speed is the avoidance speed. This process was recorded as a trail, and several trails could be obtained in each phase. We calculated the average approach-avoidance speed of each trail, which was the social approach-avoidance speed of mice. An unfamiliar CD1 mouse, a novel object (cylinder block), a familiar C57 mouse, and an unfamiliar C57 mouse were placed in the cage in turn with an interval of 10 min, during which the mice were put back into the home cage. After each phase, the apparatus was cleaned with a solution of 70% ethanol in water to remove olfactory cues, and all of the behavioral tests were conducted under red-light conditions in a room isolated from external sound sources.

Three-chamber test

Social behavior was measured using the three-chamber social interaction chamber as previously described. The apparatus was composed of rectangular, three-chamber boxes (63 cm by 45 cm by 45 cm). Each dividing wall had an open middle section, which allowed free access to each chamber. Two identical plastic cups were placed in each side chamber. Animal behaviors were scored 3 weeks after surgery and virus injection. Before behavioral testing, the test mouse was moved to a holder cage, and the fiber optic cannula was connected to the fiber optic patch cord. The social behavior test comprised two parts: a habituation session and a trial session. During the habituation session, two empty wire cages were placed in the left and right chambers. The test mouse was placed in the middle chamber and allowed to explore all three chambers of the apparatus for 5 min. The doors to the side chambers were closed, and the test mouse was placed in the middle chamber. Doors between chambers were opened to allow the test mouse to explore the three chambers freely. The test C57 mouse was allowed to explore for a trial session for 5 min. The three-chamber test was composed of three phases with 10-min intervals between each phase. After each phase, the apparatus was cleaned with a solution of 70% ethanol in water to remove olfactory cues, and all of the behavioral tests were conducted under red-light conditions in a room isolated from external sound sources. In the first phase, the two side cages were randomly placed with an unfamiliar CD1 mouse versus an empty cage. Then, a three-chamber test with a familiar C57 mouse versus an unfamiliar object was used to measure sociability, and a three-chamber test with a familiar C57 mouse versus an unfamiliar C57

mouse was used to measure the social novelty preference of mice (*2*). In the sociability phase, the two side cages were randomly placed with a familiar C57 mouse versus a novel object. In the social novelty phase, the two side cages were randomly placed with a familiar C57 mouse versus an unfamiliar C57 mouse. In the first (habituation) phase, the social preference index was calculated by the following formula: (time spent in compartment with an unfamiliar CD1 mouse − time spent in compartment with empty cage)/(time spent in compartment with an unfamiliar CD1 mouse + time spent in compartment with empty cage). In the sociability phase, the social preference index was calculated by the following formula: (time spent in compartment with a familiar C57 mouse − time spent in compartment with a novel object)/(time spent in compartment with a familiar C57 mouse + time spent in compartment with a novel object). In the social novelty phase, the social novelty index was calculated by the following formula: (time spent in compartment with an unfamiliar C57 mouse − time spent in compartment with a familiar C57 mouse)/(time spent in compartment with an unfamiliar C57 mouse + time spent in compartment with a familiar C57 mouse).

Open-field test

To test whether the circuit would affect mouse locomotion, we used an OFT as described previously. Briefly, the animals were placed individually in the center of a homemade open-field chamber (50 cm by 50 cm by 30 cm) and allowed to explore for 10 min under dim light. The open-field chamber was thoroughly cleaned with 70% ethanol before each session. Behavior was recorded by a video camera (frame rate, 30 Hz) placed above the chamber. Only pre-session and opto-session were conducted in this test. Total locomotion distance and speed were analyzed automatically by ANY-maze.

Tail suspension test

TST was performed as previously described. Briefly, mice were suspended from their tails using adhesive tape and video-recorded for 6 min. A plastic centrifuge tube with the bottom end cut off was placed over the tail to prevent mice from climbing their tails during the test. Three mice were tested simultaneously with an opaque screen separating them. Videos were scored offline for immobility blind to treatment. Only pre-session and opto-session were conducted in this test. All data during these phases were automatically recorded by ANY-maze software.

Real-time position preference

On a baseline (pretest) day, mice were placed on the border between two adjoining (20 cm by 20 cm) homogeneous gray compartments, and the amount of time spent in each compartment was recorded using video tracking software (ANY-maze). Most mice displayed no preference, and only those with >75% side preference on the pretest were excluded from further study. On the subsequent day, one side was designated active, and entry to the active side triggered opto-stimulation (20 Hz, 10-ms pulse, 10 mW), using the lasers as described above but controlled by an ANY-maze interface. Sessions lasted for 20 min, and the amount of time spent in each compartment, distance traveled, speed, and number of crossings were recorded.

Novelty-suppressed feeding test

The apparatus consisted of a plastic box (50 cm by 50 cm by 20 cm), and a fluorescent light (450 lux) was placed at the center of the arena. The floor was covered with approximately 2 cm of wooden bedding, and the animals were deprived of food for 24 hours before the test. A single pellet of food (regular chow) on a white paper platform was placed at the center of the box. Mice were placed respectively in a corner of the maze while a stopwatch was immediately started. The assessment of interest (chewing) was scored when the mouse was sitting on its haunches and biting food with the use of forepaws. The mice were moved to their home cage immediately after the test. The amount of food consumed within 6 min (food consumption in home cage) was measured.

RNA-seq analysis

RNA-seq experimental procedure. Total RNA was extracted using the mirVana miRNA Isolation Kit (Ambion, Shanghai, China) following the manufacturer's protocol. RNA integrity was evaluated using the Agilent 2100 Bioanalyzer (Agilent Technologies, Santa Clara, USA). The samples with RNA integrity number ≥7 were subjected to the subsequent analysis. The libraries were constructed using the TruSeq Stranded mRNA LTSample Prep Kit (Illumina, San Diego, USA) according to the manufacturer's instructions. Then, these libraries were sequenced on the Illumina sequencing platform (HiSeqTM 2500 or Illumina HiSeq X Ten), and 125–base pair (bp)/150-bp paired-end reads were generated. Quality control and mapping raw data (raw reads) were processed using Trimmomatic. The reads containing poly-N and the low-quality reads were removed to obtain the clean reads. Then, the clean reads were mapped to reference genome using HISAT2.

RNA-seq bioinformatic analysis. Gene-level quantification, analysis of differentially expressed genes (DEGs), cluster analysis, GO and Kyoto Encyclopedia of Genes and Genomes (KEGG) enrichment, and fragments per kilobase million (FPKM) value of each gene were calculated using Cufflinks, and the read counts of each gene were obtained by htseq-count. DEGs were identified using the DESeq (2012) R package functions estimateSizeFactors and nbinomTest. $P < 0.05$ and fold change > 2 or fold change < 0.5 were set as the threshold for significantly differential expression. Hierarchical cluster analysis of DEGs was performed to explore gene expression pattern. GO enrichment and KEGG pathway enrichment analysis of DEGs were performed respectively using R based on the hypergeometric distribution.

Transcript-level quantification, analysis of DEGs, cluster analysis, GO and KEGG enrichment, and FPKM and read count value of each transcript (protein coding) were calculated using bowtie2 and eXpress. DEGs were identified using the DESeq (2012) functions estimate Size Factors and nbinomTest. $P < 0.05$ and fold change > 2 or fold change < 0.5 were set as the threshold for significantly differential expression. Hierarchical cluster analysis of DEGs was performed to explore transcript expression pattern. GO enrichment and KEGG pathway enrichment analysis of DEGs were performed respectively using R based on the hypergeometric distribution.

Quantitative real-time PCR. For quantitative real-time polymerase chain reaction (qRT-PCR), we used 10 μl of SsoFast EvaGreen Supermix per reaction (Bio-Rad Laboratories), 0.8 μl of primer (10 μM), and 1 μl of complementary DNA in a Bio-Rad CFX96 real-time PCR detection system using the following protocol: 95°C for 30 s, 39 cycles of 95°C for 5 s, and 57°C for 5 s. In addition, the Bio-Rad Prime PCR SYBR Green assay was used to measure the expression of β-actin together with the positive control assay (qHsaCtlD0001003) according to the manufacturer's protocol (Bio-Rad Laboratories, Hercules, CA, USA). Analysis was performed using the ΔΔCT method with β-actin (*Actb*) as the calibrator gene. Primer sequences are shown in table S3.

RNA-seq data analysis. All the raw data were smoothed with a moving average filter (five-point span) and then segmented and

aligned according to the onset of social interaction within individual trials or bouts. The fluorescence change ($\Delta F/F$) values were calculated as $(F - F_0)/F_0$, where F_0 is the baseline fluorescence signals averaged over a 2-s-long control time window (typically set as 1 s) before a trigger event. To compare activity between different groups, bar graphs were computed by averaging data along a 0.5-s time window centered on the time of the activity pic. Time courses were made by averaging individual trials aligned to the time of interaction. A multivariate permutation (1000 permutations, α level of 0.05) test was used to account for data significance level on time courses, and a threshold indicating a statistically significant increase from the baseline was applied ($P < 0.005$) (*49*). Areas surrounding the time courses and error bars represent means ± SEM.

Quantification and statistical analysis

Data were expressed as the means ± SEM and analyzed using SPSS 18.0 software (SPSS, Chicago, USA). In all behavioral assays, subjects were randomly assigned to several groups, and the experiments were performed blind to genotype or treatment. The estimates of the necessary sample size (s) required were based on statistical criteria. Statistical analyses were performed using unpaired Student's *t* tests, one- or two-way analysis of variance (ANOVA), or repeated-measures ANOVA, where appropriate. Significant effects in ANOVA were followed by Bonferroni's post hoc multiple comparison tests. Post hoc significance values were set as $P < 0.05$, $P < 0.01$, and $P < 0.001$. All statistical tests used are indicated in the figure legends.

SUPPLEMENTARY MATERIALS

Supplementary material for this article is available at https://science.org/doi/10.1126/sciadv.abe8828

View/request a protocol for this paper from *Bio-protocol*.

REFERENCES AND NOTES

1. C. S. Gabor, A. Phan, A. E. Clipperton-Allen, M. Kavaliers, E. Choleris, Interplay of oxytocin, vasopressin, and sex hormones in the regulation of social recognition. *Behav. Neurosci.* **126**, 97–109 (2012).
2. S. S. Moy, J. J. Nadler, A. Perez, R. P. Barbaro, J. M. Johns, T. R. Magnuson, J. Piven, J. N. Crawley, Sociability and preference for social novelty in five inbred strains: An approach to assess autistic-like behavior in mice. *Genes Brain Behav.* **3**, 287–302 (2004).
3. H. Y. Meltzer, P. A. Thompson, M. A. Lee, R. Ranjan, Neuropsychologic deficits in schizophrenia: Relation to social function and effect of antipsychotic drug treatment. *Neuropsychopharmacology* **14**, 27S–33S (1996).
4. J. H. Kogan, P. W. Frankland, A. J. Silva, Long-term memory underlying hippocampus-dependent social recognition in mice. *Hippocampus* **10**, 47–56 (2000).
5. T. Raam, K. M. McAvoy, A. Besnard, A. H. Veenema, A. Sahay, Hippocampal oxytocin receptors are necessary for discrimination of social stimuli. *Nat. Commun.* **8**, 2001 (2017).
6. M. C. Chiang, A. J. Y. Huang, M. E. Wintzer, T. Ohshima, T. J. McHugh, A role for CA3 in social recognition memory. *Behav. Brain Res.* **354**, 22–30 (2018).
7. M. L. Donegan, F. Stefanini, T. Meira, J. A. Gordon, S. Fusi, S. A. Siegelbaum, Coding of social novelty in the hippocampal CA2 region and its disruption and rescue in a 22q11.2 microdeletion mouse model. *Nat. Neurosci.* **23**, 1365–1375 (2020).
8. J. M. Finlay, G. A. Dunham, A. M. Isherwood, C. J. Newton, T. V. Nguyen, P. C. Reppar, I. Snitkovski, S. A. Paschall, R. W. Greene, Effects of prefrontal cortex and hippocampal NMDA NR1-subunit deletion on complex cognitive and social behaviors. *Brain Res.* **1600**, 70–83 (2015).
9. O. Kampman, M. Viikki, K. Jarventausta, E. Leinonen, Meta-analysis of anxiety disorders and temperament. *Neuropsychobiology* **69**, 175–186 (2014).
10. C. Li, Y. Yan, J. Cheng, G. Xiao, J. Gu, L. Zhang, S. Yuan, J. Wang, Y. Shen, Y. D. Zhou, Toll-like receptor 4 deficiency causes reduced exploratory behavior in mice under approach-avoidance conflict. *Neurosci. Bull.* **32**, 127–136 (2016).
11. B. A. Gasser, J. Kurz, W. Senn, G. Escher, M. G. Mohaupt, Stress-induced alterations of social behavior are reversible by antagonism of steroid hormones in C57/BL6 mice. *Naunyn Schmiedebergs Arch. Pharmacol.* **394**, 127–135 (2021).
12. A. R. Burke, C. M. McCormick, S. M. Pellis, J. L. Lukkes, Impact of adolescent social experiences on behavior and neural circuits implicated in mental illnesses. *Neurosci. Biobehav. Rev.* **76**, 280–300 (2017).
13. J. van Honk, P. A. Bos, D. Terburg, S. Heany, D. J. Stein, Neuroendocrine models of social anxiety disorder. *Dialogues Clin. Neurosci.* **17**, 287–293 (2015).
14. C. Garcia-Diaz, M. J. Sanchez-Catalan, E. Castro-Salazar, A. Garcia-Aviles, H. Albert-Gasco, S. Sanchez-Sarasua de la Barcena, A. M. Sanchez-Perez, A. L. Gundlach, F. E. Olucha-Bordonau, Nucleus incertus ablation disrupted conspecific recognition and modified immediate early gene expression patterns in 'social brain' circuits of rats. *Behav. Brain Res.* **356**, 332–347 (2019).
15. Y. T. Lin, C. C. Chen, C. C. Huang, K. Nishimori, K. S. Hsu, Oxytocin stimulates hippocampal neurogenesis via oxytocin receptor expressed in CA3 pyramidal neurons. *Nat. Commun.* **8**, 537 (2017).
16. H. W. Suh, H. K. Lee, Y. J. Seo, M. S. Kwon, E. J. Shim, J. Y. Lee, S. S. Choi, J. H. Lee, Kainic acid (KA)-induced Ca2+/calmodulin-dependent protein kinase II (CaMK II) expression in the neurons, astrocytes and microglia of the mouse hippocampal CA3 region, and the phosphorylated CaMK II only in the hippocampal neurons. *Neurosci. Lett.* **381**, 223–227 (2005).
17. M. K. Chawla, V. L. Sutherland, K. Olson, B. L. McNaughton, C. A. Barnes, Behavior-driven arc expression is reduced in all ventral hippocampal subfields compared to CA1, CA3, and dentate gyrus in rat dorsal hippocampus. *Hippocampus* **28**, 178–185 (2018).
18. J. X. Jiang, H. Liu, Z. Z. Huang, Y. Cui, X. Q. Zhang, X. L. Zhang, Y. Cui, W. J. Xin, The role of CA3-LS-VTA loop in the formation of conditioned place preference induced by context-associated reward memory for morphine. *Addict. Biol.* **23**, 41–54 (2018).
19. A. G. Ophir, Navigating monogamy: Nonapeptide sensitivity in a memory neural circuit may shape social behavior and mating decisions. *Front. Neurosci.* **11**, 397 (2017).
20. S. Shin, H. Pribiag, V. Lilascharoen, D. Knowland, X. Y. Wang, B. K. Lim, Drd3 signaling in the lateral septum mediates early life stress-induced social dysfunction. *Neuron* **97**, 195–208.e6 (2018).
21. K. V. Sandhu, Y. E. Demiray, Y. Yanagawa, O. Stork, Dietary phytoestrogens modulate aggression and activity in social behavior circuits of male mice. *Horm. Behav.* **119**, 104637 (2020).
22. A. Bilella, G. Alvarez-Bolado, M. R. Celio, Coaxiality of Foxb1- and parvalbumin-expressing neurons in the lateral hypothalamic PV1-nucleus. *Neurosci. Lett.* **566**, 111–114 (2014).
23. G. Alvarez-Bolado, M. R. Celio, The ventrolateral hypothalamic area and the parvafox nucleus: Role in the expression of (positive) emotions? *J. Comp. Neurol.* **524**, 1616–1623 (2016).
24. A. Bilella, G. Alvarez-Bolado, M. R. Celio, The Foxb1-expressing neurons of the ventrolateral hypothalamic parvafox nucleus project to defensive circuits. *J. Comp. Neurol.* **524**, 2955–2981 (2016).
25. I. Toth, I. D. Neumann, Animal models of social avoidance and social fear. *Cell Tissue Res.* **354**, 107–118 (2013).
26. A. J. Lopez, E. Kramar, D. P. Matheos, A. O. White, J. Kwapis, A. Vogel-Ciernia, K. Sakata, M. Espinoza, M. A. Wood, Promoter-specific effects of DREADD modulation on hippocampal synaptic plasticity and memory formation. *J. Neurosci.* **36**, 3588–3599 (2016).
27. J. T. Zhang, Y. Liu, L. X. Li, K. Li, J. G. Chen, F. Wang, Activation of EphB2 in the basolateral amygdala promotes stress vulnerability of mice by increasing NMDA-dependent synaptic function. *Neuropharmacology* **167**, 107934 (2020).
28. L. C. Wong, L. Wang, J. A. D'Amour, T. Yumita, G. Chen, T. Yamaguchi, B. C. Chang, H. Bernstein, X. You, J. E. Feng, R. C. Froemke, D. Lin, Effective modulation of male aggression through lateral septum to medial hypothalamus projection. *Curr. Biol.* **26**, 593–604 (2016).
29. C. Silva, N. McNaughton, Are periaqueductal gray and dorsal raphe the foundation of appetitive and aversive control? A comprehensive review. *Prog. Neurobiol.* **177**, 33–72 (2019).
30. T. Zhao, X. Zhou, N. Szabo, M. Leitges, G. Alvarez-Bolado, Foxb1-driven Cre expression in somites and the neuroepithelium of diencephalon, brainstem, and spinal cord. *Genesis* **45**, 781–787 (2007).
31. W. Han, L. A. Tellez, M. H. Perkins, I. O. Perez, T. Qu, J. Ferreira, T. L. Ferreira, D. Quinn, Z. W. Liu, X. B. Gao, M. M. Kaelberer, D. V. Bohorquez, S. J. Shammah-Lagnado, G. de Lartigue, I. E. de Araujo, A neural circuit for gut-induced reward. *Cell* **175**, 665–678.e23 (2018).
32. K. Deng, L. Yang, J. Xie, H. Tang, G. S. Wu, H. R. Luo, Whole-brain mapping of projection from mouse lateral septal nucleus. *Biol. Open* **8**, bio043554 (2019).
33. C. C. Young, M. Stegen, R. Bernard, M. Muller, J. Bischofberger, R. W. Veh, C. A. Haas, J. Wolfart, Upregulation of inward rectifier K+ (Kir2) channels in dentate gyrus granule cells in temporal lobe epilepsy. *J. Physiol.* **587**, 4213–4233 (2009).
34. R. Bartesaghi, M. Raffi, E. Ciani, Effect of early isolation on signal transfer in the entorhinal cortex-dentate-hippocampal system. *Neuroscience* **137**, 875–890 (2006).
35. T. Okuyama, T. Kitamura, D. S. Roy, S. Itohara, S. Tonegawa, Ventral CA1 neurons store social memory. *Science* **353**, 1536–1541 (2016).

36. R. Menon, T. Grund, I. Zoicas, F. Althammer, D. Fiedler, V. Biermeier, O. J. Bosch, Y. Hiraoka, K. Nishimori, M. Eliava, V. Grinevich, I. D. Neumann, Oxytocin signaling in the lateral septum prevents social fear during lactation. *Curr. Biol.* **28**, 1066–1078.e6 (2018).
37. I. Zoicas, D. A. Slattery, I. D. Neumann, Brain oxytocin in social fear conditioning and its extinction: Involvement of the lateral septum. *Neuropsychopharmacology* **39**, 3027–3035 (2014).
38. Y. F. Guzman, N. C. Tronson, V. Jovasevic, K. Sato, A. L. Guedea, H. Mizukami, K. Nishimori, J. Radulovic, Fear-enhancing effects of septal oxytocin receptors. *Nat. Neurosci.* **16**, 1185–1187 (2013).
39. F. Leroy, J. Park, A. Asok, D. H. Brann, T. Meira, L. M. Boyle, E. W. Buss, E. R. Kandel, S. A. Siegelbaum, A circuit from hippocampal CA2 to lateral septum disinhibits social aggression. *Nature* **564**, 213–218 (2018).
40. A. Benoy, A. Dasgupta, S. Sajikumar, Hippocampal area CA2: An emerging modulatory gateway in the hippocampal circuit. *Exp. Brain Res.* **236**, 919–931 (2018).
41. S. J. Middleton, T. J. McHugh, CA2: A highly connected intrahippocampal relay. *Annu. Rev. Neurosci.* **43**, 55–72 (2020).
42. M. J. Millan, The neurobiology and control of anxious states. *Prog. Neurobiol.* **70**, 83–244 (2003).
43. B. Lange, P. Pauli, Social anxiety changes the way we move—A social approach-avoidance task in a virtual reality CAVE system. *PLOS ONE* **14**, e0226805 (2019).
44. C. J. Smith, K. B. Wilkins, J. N. Mogavero, A. H. Veenema, Social novelty investigation in the juvenile rat: Modulation by the μ-opioid system. *J. Neuroendocrinol.* **27**, 752–764 (2015).
45. D. Enter, P. Spinhoven, K. Roelofs, Alleviating social avoidance: Effects of single dose testosterone administration on approach-avoidance action. *Horm. Behav.* **65**, 351–354 (2014).
46. A. Pittig, K. Hengen, F. Bublatzky, G. W. Alpers, Social and monetary incentives counteract fear-driven avoidance: Evidence from approach-avoidance decisions. *J. Behav. Ther. Exp. Psychiatry* **60**, 69–77 (2018).
47. H. Wang, Y. Z. Tan, R. H. Mu, S. S. Tang, X. Liu, S. Y. Xing, Y. Long, D. H. Yuan, H. Hong, Takeda G protein-coupled receptor 5 modulates depression-like behaviors via hippocampal CA3 pyramidal neurons afferent to dorsolateral septum. *Biol. Psychiatry* **89**, 1084–1095 (2021).
48. F. Leichsenring, F. Leweke, Social anxiety disorder. *N. Engl. J. Med.* **376**, 2255–2264 (2017).
49. Z. Zhou, X. Liu, S. Chen, Z. Zhang, Y. Liu, Q. Montardy, Y. Tang, P. Wei, N. Liu, L. Li, R. Song, J. Lai, X. He, C. Chen, G. Bi, G. Feng, F. Xu, L. Wang, A VTA GABAergic neural circuit mediates visually evoked innate defensive responses. *Neuron* **103**, 473–488.e6 (2019).
50. D. Chaudhury, J. J. Walsh, A. K. Friedman, B. Juarez, S. M. Ku, J. W. Koo, D. Ferguson, H. C. Tsai, L. Pomeranz, D. J. Christoffel, A. R. Nectow, M. Ekstrand, A. Domingos, M. S. Mazei-Robison, E. Mouzon, M. K. Lobo, R. L. Neve, J. M. Friedman, S. J. Russo, K. Deisseroth, E. J. Nestler, M. H. Han, Rapid regulation of depression-related behaviours by control of midbrain dopamine neurons. *Nature* **493**, 532–536 (2013).

Acknowledgments: We thank M.-H. Han (Mount Sinai School of Medicine) for suggestions on the experimental design. We thank H. Zhang (Cleveland Clinic Foundation) for technical support and suggestions and J.-T. Zhang (Qingdao Center Hospital) for suggestions on data statistics and schematic drawing. We thank S.-Q. Gao for supporting us during schematic drawing. **Funding:** This work was supported by grants from the National Key R&D Program of China (2021ZD0202900), the Innovative Research Groups of National Natural Scientific Foundation of China (nos. 81721005 to J.-G.C.), the National Natural Science Foundation of China (nos. 82130110 and 81973310 to J.-G.C.; nos. U21A20363 and 81971279 to F.W.), and the Program for Changjiang Scholars and Innovative Research Team Grant (no. IRT13016 to J.-G.C.). **Author contributions:** Y.L., F.W., and J.-G.C. designed the experiments. S.-L.D. and Q.L. performed in vitro patch-clamp recording. S.-L.D., Q.L., Y.L., and L.-X.L. performed the fluorescence in immunohistochemistry. Y.L. and L.-X.L. performed the CSDS training and social behavioral test. Y.L. and L.-X.L. conducted the fiber photometry and behavior test. Y.L., L.-X.L., Q.L., Z.-Y.W., and Z.-X.Z. performed the stereotaxic surgery and microinjection of virus. Y.L. and Z.-X.Z. performed the RNA-seq experimental procedure and bioinformatic analysis. Y.L. and Z.-X.Z. performed the qRT-PCR. Y.L., Z.-X.Z., L.-X.L., and S.-L.D. performed PRV labeling. Y.L. performed statistical analyses. Y.L. wrote the paper with the assistance of F.W. and J.-G.C. **Competing interests:** The authors declare that they have no competing interests. **Data and materials availability:** All data needed to evaluate the conclusions in the paper are present in the paper and/or the Supplementary Materials.

Submitted 27 September 2020
Accepted 29 December 2021
Published 23 February 2022
10.1126/sciadv.abe8828